Fluid mechanics of air recycling and filtration for indoor airborne transmission (2) (3)

Cite as: Phys. Fluids **35**, 013344 (2023); https://doi.org/10.1063/5.0135718 Submitted: 22 November 2022 • Accepted: 29 December 2022 • Accepted Manuscript Online: 06 January 2023 • Published Online: 30 January 2023

🧓 K. A. Krishnaprasad, 🔟 J. S. Salinas, 🔟 N. Zgheib, et al.

COLLECTIONS

Paper published as part of the special topic on Flow and the Virus

- This paper was selected as Featured
- This paper was selected as Scilight







ARTICLES YOU MAY BE INTERESTED IN

Tracking airborne nuclei to determine air filtration efficacy in reducing viral spread Scilight 2023, 051101 (2023); https://doi.org/10.1063/10.0017158

Dynamic kirigami structures for wake flow control behind a circular cylinder Physics of Fluids 35, 011707 (2023); https://doi.org/10.1063/5.0130369

Steady three-dimensional unbounded flow past an obstacle continuously deviating from a sphere to a cube

Physics of Fluids 35, 013343 (2023); https://doi.org/10.1063/5.0133499





Fluid mechanics of air recycling and filtration for indoor airborne transmission (1) (2)

Cite as: Phys. Fluids **35**, 013344 (2023); doi: 10.1063/5.0135718 Submitted: 22 November 2022 · Accepted: 29 December 2022 · Published Online: 30 January 2023















AFFILIATIONS

Note: This paper is part of the special topic, Flow and the Virus.

a) Author to whom correspondence should be addressed: nadim.zgheib@utrgv.edu

ABSTRACT

We present a statistical framework to account for effects of recycling and filtration in ventilation systems for the estimation of airborne droplet nuclei concentration in indoor spaces. We demonstrate the framework in a canonical room with a four-way cassette air-conditioning system. The flow field within the room is computed using large eddy simulations for varying values of air changes per hour, and statistical overloading is used for droplet nuclei, which are tracked with a Langevin model accounting for sub-grid turbulence. A key element is to break up the path that a virus-laden droplet nucleus can take from the time it is ejected by the sick individual to the time it reaches the potential host into four separate elementary processes. This approach makes it possible to provide turbulence-informed and statistically relevant pathogen concentration at any location in the room from a source that can be located anywhere else in the room. Furthermore, the approach can handle any type of filtration and provides a correction function to be used in conjunction with the well-mixed model. The easy-to-implement correction function accounts for the separation distance between the sick and the susceptible individuals, an important feature that is inherently absent in the well-mixed model. The analysis shows that using proper filtration can increase the cumulative exposure time in typical classroom settings by up to four times and could allow visitations to nursing homes for up to 45 min.

Published under an exclusive license by AIP Publishing. https://doi.org/10.1063/5.0135718

I. INTRODUCTION

The fluid mechanics of airborne spreading has received (and continues to receive) ample attention in recent years as Covid-19 cases are raging around the world. 1-12 It is clearly a key component for understanding airborne spreading of contagion. Not only is it necessary for controlling the spread of airborne diseases, it is also crucial for avoiding potentially unnecessary stringent restrictions. A good understanding of the fluid mechanics of airborne transmission coupled with a good understanding of the virology and immunology aspects would guide policy makers in proposing effective mandates that provide the necessary level of protection while being minimally disruptive. 13

The risk of airborne transmission is substantially higher in poorly ventilated indoor spaces where concentration levels of the virus could exceed acceptable thresholds. 14-18 To lower the risk of airborne transmission in confined spaces, it is recommended to reduce the recycling of contaminated air by drawing in outdoor, pathogen-free air into the room in question at a relatively large ACH (air changes per hour). 19,20 While drawing in fresh, pathogen-free air without any recycling does

minimize the risk of infection, the cooling/heating cost considerations often require some portion of the air to be recycled back into the room. In the context of recycling, the risk of infection can be greatly reduced with the use of air filters, which prevents a large amount of the pathogen-carrying droplet nuclei from reentering the room. HEPA (high-efficiency particulate air) filters are known to remove over 99.97% of particles;²¹ however, due to their high cost, they may become out of reach for many schools, restaurants, and businesses. On the other hand, more affordable filters can have droplet sizedependent filtration efficiencies of only around 60%.²²

Cumulative exposure time (CET) is an important metric that is used in contact tracing as well as for developing social distancing guidelines. It is defined as the maximum safe duration a group of N potential receivers can remain in an indoor space after the arrival of one infected individual and maintain risk of infection below a set risk tolerance. 23,24 The advantage of CET is its ease of interpretation in terms of either how long it is safe to remain in an indoor space or how many people can gather in an indoor space for a set duration of time.

¹Department of Mechanical and Aerospace Engineering, University of Florida, Gainesville, Florida 32611, USA

²Department of Mechanical Engineering, The University of Texas Rio Grande Valley, Edinburg, Texas 78573, USA

b)Electronic mail: bala1s@ufl.edu

Consider the example of a canonical classroom with one teacher and several students with forced ventilation within the room with an airconditioning unit. The probability of viral contagion spreading from one sick individual to other susceptible individuals depends on various factors: (i) physiological factors, such as the ejection rates of the infected and the susceptible individuals, which depend on their activity (breathing, talking, singing, sneezing, etc.); (ii) ventilation factors, such as ACH, portion of recycled air compared to the amount of fresh air drawn from outside, the efficiency of filtration of recycled air, location of the air-conditioning inlet and outlet; (iii) virological factors, such as the viral load of the ejected droplets by the infected individual, the infectivity of the ejected viral load, the natural deactivation rate of the virus within the indoor space; and (iv) other factors, such as the location of the infected and the susceptible individuals within the room, the quality of the mask being used, etc. We then come to the conclusion that while CET is a simple measure that can be used for decision making, its effectiveness depends on how well it accounts for all the physiological, ventilation, virological, and other

One particularly simple model that has been successful in predicting CET in indoor spaces by incorporating the physiological, ventilation, virological, and other factors is the well-mixed model.² The well-mixed model has been used to estimate pathogen concentration in confined spaces, which then is used to evaluate CET. As the name implies, it assumes the pathogen, within the room in question, to be uniformly and instantaneously distributed upon ejection. Therefore, under the well-mixed assumption, as a person speaks or coughs within a room, the concentration of ejected droplets are assumed to be instantly well-mixed within the room and available at any other location with equal probability. The well-mixed model, which is also known as the well-stirred model, has been around for many decades and has been used in several contexts, including chemical reactors,²⁷ pharmaceutical industry,²⁸ combustion chambers,²⁹ and heat transfer in fluidized beds.³⁰ The model is motivated by the turbulent nature of the flow, which entails strong mixing.

The amount of air being recycled in the air-conditioning system and the efficiency of filtration of the recycled air play an important role in determining the concentration of pathogen within the indoor space. The role of recycling and filtration is clearly brought out by the following two contrasting scenarios: (i) 100% recycling of the exhaust back into the room without filtration and (ii) either no-recycling of exhaust air back into the room or perfect 100% filtration efficiency of recycled air. Consider an infected individual entering a room at t=0and ejecting airborne, virus-laden droplet nuclei at a constant rate. In the former scenario of 100% recycling without filtration, the loss of pathogen occurs solely through the natural deactivation of the virus over time and by deposition of droplet nuclei on the room walls and floor. In the second scenario, there is another powerful mechanism of pathogen loss, which entails a substantial portion of the pathogen leaving the room through the outlet and never reentering the room. Thus, pathogen concentration in a room with fully recycled air without filtration can be substantially larger compared to the concentration in a room where fresh air is being drawn from outside or the recycled air is properly filtered. In fact, it should be noted that pathogen concentration in a room with fully recycled air without filtration is nearly independent of how fast the air is being changed (i.e., independent of ACH).

One of the advantages of the well-mixed model is its simplicity and ability to take into account virological and epidemiological factors. The well-mixed model easily accounts for recycling and filtration in the prediction of the average pathogen concentration within the room. Needless to say, there are shortcomings to the well-mixed assumption. In the context of airborne transmission, the serious deficiency is its inability to account for the spatial separation between the infected individual (henceforth referred to as the source) and the susceptible individual (henceforth referred to as the sink). As a result of the assumption of instantaneous well-mixing of the pathogen, there is no difference between the source and the sink being separated by 2 or 10 m.

In a recent study, Salinas et al.²⁴ considered a canonical room of size $10 \times 10 \times 3.2 \,\mathrm{m}^3$ with a four-way cassette air-conditioning unit and performed large eddy simulations (LES) of droplet nuclei dispersion to investigate in detail and quantify departure from wellmixedness. Their detailed investigation was layered at four different levels: (i) averaging over all possible source and sink locations, i.e., the room average, (ii) averaging over all possible source locations, i.e., from the sink perspective, (iii) averaging over all possible sink locations, i.e., from the source perspective, and (iv) averaging over all possible combinations of the source and sink locations that are a specific distance apart. Their major conclusions were that the well-mixed theory can accurately predict the room-averaged concentration to within a few percent. However, for their canonical room of $10 \times 10 \times 3.2 \,\mathrm{m}^3$, the well-mixed theory under-estimates pathogen concentration by a factor of 2 to 3 when the susceptible individual is within a distance of 5 m from the infected individual. They also showed that a simple correction function applied to the well-mixed model can account for the effect of source-to-sink distance.

The above quantification of departure from the well-mixed theory was in the context of perfect filtration or zero recycling. With recycling and imperfect filtration, the air inlet into the room acts as another continuous source of pathogen entering the room, whose mixing within the room is likely to be somewhat different from the mixing of pathogens that are ejected by the source. According to the wellmixed theory, there is no difference between the pathogen ejected by the source and the pathogen reentering the room through the inlet, since both are well-mixed within the room instantly and available to one and all at equal probability. However, it has been shown that the concentration of airborne droplet nuclei ejected by the source somewhat depends on the source location within the room.²⁴ In the case of droplet nuclei reentering the room through the inlet port, it is likely that the nuclei will be more concentrated in the regions of the highly focused inlet jets. Thus, there is reason to believe that departure from well-mixedness observed in the absence of recycling may apply to situations with recycling and filtration as well. While the mixing of droplet nuclei ejected by the source is likely to be different from the mixing of droplet nuclei introduced through the inlet ports, their combined effect is additive. We exploit this superposition in the statistical description of the departure from the well-mixed theory while fully taking into account recycling and filtration.

The present goal is to systematically investigate the effects of recycling and filtration in the context of departure from the well-mixed theory. Apart from all other physiological, ventilation, and virological factors, the fraction of air being recycled and the efficiency of filtration become two additional factors that influence the probability

of infection. Our goal is to generalize the statistical framework developed in Ref. 24 so that it can be used to make predictions under conditions of recycling and filtration. The generalization will be built on the fact that the pathogen concentration at a sink location has a *direct route* due to the arrival of the nuclei from the source and an *indirect route* where the nuclei originating at the source recycle through the air conditioning unit (escaping the filter) one or more times before reaching the sink. By separating the direct and indirect routes and obtaining their statistics independently, the present analysis will investigate all possible values of recycling and filtration efficiency through superposition.

We recall that the statistical properties of the direct route from the source to the sink have been thoroughly analyzed by Salinas et al.²⁴ The first step of the present work is to consider the fate of droplet nuclei introduced into the room through the inlet ports. This step contributes to the evaluation of the statistics of viral-laden droplet nuclei traveling from the inlet to a sink located within the room. We will follow the strategy pursued by Salinas et al.24 and study the statistics of nuclei traveling from the inlet to a sink. In particular, we plan to answer the following questions: (i) when averaged over all possible source and sink locations, Salinas et al.²⁴ observed the pathogen concentration to be in excellent agreement with the well-mixed theory. Does this agreement hold even for injection of nuclei through the inlet ports, when averaged over all sink locations? (ii) How does the normalized concentration of nuclei injected at the inlet vary as a function of sink location within the room? If this variation is substantial, then a correction function is needed to account for the location of the sink with respect to the inlet ports.

The second step of the present work is to combine the results of the direct and the indirect routes and predict the pathogen concentration in the presence of recycling and filtration. This analysis will start at the level of the room average along with a comparison to the well-mixed theory. Salinas *et al.*²⁴ quantified deviation from the well-mixed theory in terms of a correction function that only depends on the source–sink distance. A similar approach will be developed in the presence of recycling and filtration with the introduction of appropriate correction functions.

In predicting the cumulative exposure time (CET), the overarching goal of the present approach is to leverage the power of the well-mixed theory. We start with the well-mixed theory as the foundation and develop an easy-to-implement correction procedure that accounts for systematic departures from well-mixedness. We extend the approach of Ref. 24 to develop a correction procedure that accounts for not only the source-to-sink separation distance but also the effects of recycling and filtration. The rest of the paper is arranged as follows. In Sec. II, we present a summary of the mathematical and numerical formulation. In Sec. III, we discuss the well-mixed model and offer statistical measures for evaluating departure from well-mixedness. In Sec. IV, we analyze the statistical properties of droplet nuclei introduced into the room from the inlet ports. In Sec. V, we lay out the proposed statistical formulation for recycling and filtration. This is followed by Sec. VI, where we separate the trajectory of the droplet nuclei into four elementary processes. In Sec. VII, we present an easy-to-implement correction function to be used in conjunction with the wellmixed model that accounts for source-sink separation distance. The correction function is then implemented in Sec. VIII in two

settings, a classroom and a nursing home. Finally, conclusions are drawn in Sec. $\rm IX$.

II. MATHEMATICAL AND NUMERICAL FORMULATION A. Gas phase

To examine the effects of recycling and filtration, we use a canonical room of size $10 \times 10 \times 3.2 \,\mathrm{m}^3$ with a typical four-way inlet surrounding a central outlet ventilation system that is located on the ceiling at the center of the room [see inset (e) of Fig. 3]. This is the same configuration as that previously studied by Salinas et al.²⁴ in the absence of recycling and filtration. The ventilation system is comprised of four inlets of size $0.055 \times 0.44 \,\mathrm{m}^2$ surrounding an outlet of size $0.6 \times 0.6 \,\mathrm{m}^2$ [see Fig. 3(e)—inlets in magenta, outlet in green]. The resolution of the entire range of turbulent length and time scales poses a great challenge. As a result, in the present work, we use large eddy simulations (LES³¹) in the context of an Euler-Lagrange point particle approach. 32,33 Two simulations are considered for which the air properties are fixed at $\rho_f = 1.2041 \text{ kg/m}^3$ and $\mu_f = 1.81$ $\times 10^{-5}$ N s/m² for the density and viscosity, respectively. The air is ejected at one of two speeds, either 3.57 or 7.14 m/s. These air speeds result in ACH values of 2.5 and 5, respectively, for which the corresponding inlet Reynolds number, $Re_{in} = 4\rho_f U_{in} A_{in}/\mu_f$, becomes approximately 23 000 and 46 000, respectively.

The gas-phase governing equations are the filtered incompressible Navier-Stokes equations, which have been rigorously derived in the context of Euler-Lagrange multiphase flow simulations. 34,35 The filtering process of the momentum equation introduces a sub-grid Reynolds stress term, which has been closed with the eddy viscosity model, where the turbulent eddy viscosity is obtained using the dynamic Smagorinsky model.^{36,37} These equations are solved using a highly scalable spectral element solver.³⁸ The domain is discretized using 60 \times 60 \times 16 hexahedral elements with 6³ Gauss-Lobatto- Legendre (GLL) grid points within each element, which results in a total of 12.4 \times 10⁶ grid points. A Dirichlet boundary condition for velocity is imposed at the inlet planes [see Fig. 3(e)], while an open boundary condition is used at the outlet.³⁹ No-slip and no penetration conditions are used at the lateral walls, floor, and ceiling. The turbulent flow is allowed to reach a statistically steady state before introducing nuclei to the simulation. For more details, we refer the reader to Salinas et al.²

We should note here that the droplet nuclei are "one-way coupled" in the sense that the air flow modifies the trajectory of the nuclei, but the nuclei do not modify the surrounding air flow. Furthermore, nuclei-nuclei collisions are neglected, and nuclei are assumed to have deposited on a surface upon impact, i.e., the collision of a droplet nucleus with a solid surface results in the nucleus depositing on the surface at the place of collision. Furthermore, we note that the present simulations are intended to track the droplet nuclei that remain airborne following an expiratory event at a time when the liquid water that make up the majority of the ejected droplets has evaporated. In other words, the present simulations are not intended to track droplets from the time of ejection when they are still laden with liquid water. In fact, the statistical overloading approach that is at the core of the present analysis is only valid in the context of very small nuclei volume fraction where one-way coupling is appropriate. The present simulations are considered room-scale simulations whose initial condition can be obtained from ejection-scale simulations and experiments.^{8,40}

B. Droplet nuclei

Each lth nuclei is individually tracked with the following governing equations:

$$\frac{\mathrm{d}}{\mathrm{d}t} \begin{bmatrix} \mathbf{X}_l \\ \mathbf{V}_l \end{bmatrix} = \begin{bmatrix} \mathbf{V}_l \\ \mathbf{F}_l/m_l \end{bmatrix}. \tag{1}$$

Here, $m_l = 4\pi r_l^3 \rho_p/3$ is the mass of the *l*th nucleus, where the radius of the nucleus is r_l with density $\rho_p = 1000 \text{ kg/m}^3$. The total force \mathbf{F}_l acting on the *l*th nucleus is computed as

$$\mathbf{F}_{l} = \mathbf{F}_{qs,l} + \mathbf{F}_{g,l} = 6\pi\mu_{f}r_{l}(\mathbf{u}(\mathbf{X}_{l}) - \mathbf{V}_{l})\Phi(\mathrm{Re}_{l}) + V_{l}(\rho_{p} - \rho_{f})|\bar{\mathbf{g}}|,$$
(2)

where $\mathbf{F}_{qs,l}$ and $\mathbf{F}_{g,l}$ are the quasi-steady and gravity-buoyancy forces, respectively. Note that in the present dilute two-phase flow, direct (collision) and indirect (fluid-mediated) interactions within the dispersed phase can be neglected. In Eq. (2), $V_l = 4\pi r_l^3/3$ is the volume of the lth nucleus, while the Reynolds number of the lth nucleus is computed as $\mathrm{Re}_l = 2\rho_f |\mathbf{u}(\mathbf{X}_l) - \mathbf{V}_l| r_l/\mu_f$, and the function $\Phi(\mathrm{Re}_l) = 1 + 0.15\mathrm{Re}_l^{0.687}$ is the finite Reynolds number drag correction.

Since we have filtered the effect of eddies smaller than the grid size, the fluid velocity u evaluated at the nucleus center requires an additional contribution from unresolved sub-grid eddies. The fluid velocity u can be computed as $\mathbf{u}(\mathbf{X}_l) = \tilde{\mathbf{u}}(\mathbf{X}_l) + \mathbf{u}'(\mathbf{X}_l)$, where the resolved part $\tilde{\mathbf{u}}$ reflects the macroscale flow computed in the LES, and \mathbf{u}' is the contribution from the unresolved sub-grid eddies. The perturbation velocity is computed using the Langevin model. For specific details on its implementation, please refer to Salinas $et\ al.^{24}$ For nuclei smaller than 10 μ m, inertial effects are negligible, and the equilibrium-Eulerian model is used, where the nuclei velocities are obtained as the superposition of the fluid velocity at the nucleus center $\mathbf{u}(\mathbf{X}_l)$ and the nucleus settling velocity.

The results from five LES simulations are used in the present analysis. In the first three LES simulations, 20×10^6 nuclei of ten different radii, ranging from 100 nm to 25 μ m, are initially randomly distributed within the room with uniform probability. The nuclei are then transported by the flow (ACH 10, 5, and 2.5), where they would eventually settle to the floor, deposit on the walls and ceiling or be removed by the outlet. For the other two simulations, 5×10^6 droplets are injected into the room through the inlet ports at ACH 5 and 2.5. The droplet nuclei trajectories are solved using the highly scalable point-particle library ppiclF. 53

It is important to note that the droplets ejected by the infected individual are taken to rapidly evaporate to their final fully evaporated droplet nuclei state within a second or so after ejection, ^{42,54–57} irrespective of the mode of ejection (speaking, singing, etc.). As a result, the present room-scale simulations consider only the dispersion of the fully evaporated airborne droplet nuclei. Furthermore, we also assume the viral load to be proportional to the volume of the droplet nuclei. ⁵⁸

III. WELL-MIXED MODEL

We consider a general configuration of a rectangular cuboidal room of volume \mathscr{V} with an air inflow rate of Q m³/s into the room and equal outflow exiting the room. In this work, we will consider two different pathways of pathogen entering the room. The first pathway consists of an infected person (source) located within the room with an exhalation rate of Q_b . Let $n_V(r)$ be the concentration of exhaled

virus-laden droplet nuclei of radius r that remain airborne such that the rate of influx of nuclei of radius r into the room is $Q_b n_V(r)$. In the second pathway, let the air entering the room be contaminated with a virus-laden droplet nuclei concentration of $n_S(r)$ such that the resulting rate of influx of nuclei of radius r into the room is $Q n_S(r)$. In the aforementioned definitions, and in the remainder of the paper, a subscript/superscript V pertains to an infected source within the V0 lume of the room and subscript/superscript V0 pertains to an influx through the V1 pertains to an influx through the V2 pertains to an influx through the V3 pertains to an influx through the V3 pertains to an influx through the V4 pertains to an influx through the V5 pertains to an influx through the V6 pertains the

In the well-mixed theory, the nuclei concentration within the room is assumed to be spatially uniform, and the time evolution of the well-mixed concentration $n_{wm}(t,r)$ of droplet nuclei of radius r is given by

$$\mathcal{V}\frac{dn_{wm}}{dt} = Q_b n_{so}(r) + Qn_{in}(r) - \mathcal{V}\lambda_{wm} n_{wm}, \qquad (3)$$

where the first two terms on the right-hand side account for the influx of the droplet nuclei of radius r from the infectious source and through the inlet, respectively, and the last term accounts for the removal of the droplet nuclei by the combined mechanisms of exit through the outlet, settling down on the floors, deposition on the walls, and natural deactivation.

Pathogen influx from an infected individual: Let us now consider the scenario where the influx is only from the volume source, and let the infected person enter the room at t=0. Also, assume the surface influx through the inlet ports to be zero (i.e., $n_S=0$). In this scenario, the droplet nuclei concentration within the room is zero before the arrival of the infected source and increases steadily over time after the arrival to reach the steady-state value. We define the normalized well-mixed nuclei concentration within the room as $\hat{n}_{wm}^V(t,r)=n_{wm}(t,r)/(Q_bn_V(r))$, where the superscript V indicates the influx being from within the volume and the normalization with respect to the ejection rate of this source. The normalization has the advantage that it removes the dependence on the details of the expiration activity of the source. The time evolution of normalized well-mixed nuclei concentration is expressed as $^{23-26,59}$

$$\hat{n}_{wm}^{V}(t,r) = \frac{1}{\lambda_{wm}(r)\mathscr{V}} \left[1 - e^{-\lambda_{wm}(r)t}\right],\tag{4}$$

where the exponential rate is given by

$$\lambda_{wm}(r) = \frac{Q}{\psi} + \frac{V_s(r)}{H} + \lambda_{dep}(r) + \lambda_{da}. \tag{5}$$

The first term on the right-hand side can be written in terms of ACH, since ACH/3600 = Q/V. The second term on the right-hand side corresponds to the decay rate due to gravitational settling of the nuclei onto the floor of the room, where $V_s(r)$ and H represent the size-dependent droplet settling velocity and room height, respectively. The third term corresponds to the loss of droplet nuclei due to their turbulent deposition on the walls and ceiling of the room, which is typically a weak mechanism of removal.²⁴ In the last term on the right-hand side, we have included the effect of deactivation of the virus over time, and this effect has been quantified as the deactivation rate $\lambda_{da}(r)$, which in general can depend on nuclei size.²³

Pathogen influx from inlet ports: Let us now consider the scenario where the influx of pathogen is only through the inlet ports (i.e., the influx from within the room is $Q_b=0$) and that the influx starts at t=0. In this scenario as well, the droplet nuclei concentration within

the room is zero for t < 0 and increases steadily over time to reach the steady-state value. We now define the normalized well-mixed nuclei concentration within the room as $\hat{n}_{wm}^S(t,r) = n_{wm}(t,r)/(Qn_S(r))$, where the superscript S indicates normalization with respect to the surface influx through the inlet ports. The time evolution of $\hat{n}_{wm}^S(t,r)$ is again given by the right-hand side of (4), since, according to the well-mixed model, there is no difference between the two scenarios. Irrespective of whether the influx of pathogen is from the infected individual or through the inlet ports, when normalized by the injection rate, the well-mixed concentration within the room remains the same.

Pathogen influx both from an infected individual and inlet ports: We now consider the scenario of pathogen influx both directly from the infected individual and from the inlet air stream. However, we will restrict the influx through the inlet ports to be the result of recycling and imperfect filtration. A portion of the inflow, Q_{nr} is considered to be new air from outside and the rest $Q_r = Q - Q_{nr}$ is recycled into the room from the outflow exiting the room. Filtration efficiency $\eta_f(r)$ is defined as the fraction of droplet nuclei of radius r that is removed from the air stream while it passes through the filter. In other words, a fraction $1 - \eta_f(r)$ of the droplet nuclei that went into the filter find their way back into the room. According to the well-mixed model, the concentration of nuclei of radius r, measured as the number of nuclei per volume of air, per nuclei size, exiting the room in the outflow stream is given by the well-mixed concentration $n_{wm}(t,r)$. Then, the concentration of nuclei of radius r entering the room in the inflow stream as a result of recycling and filtration is given by

$$n_S(t,r) = n_{wm}(t,r) \frac{Q_r}{Q} (1 - \eta_f(r)).$$
 (6)

Although there are two streams of influx of pathogens into the room, the true origin of pathogens is from the infected source. Therefore, we normalize the well-mixed nuclei concentration within the room as $\hat{n}_{wm}^{VS}(t,r) = n_{wm}(t,r)/(Q_b n_{so}(r))$, where the superscript VS indicates the combined influx both from within the volume and through the surface inlet ports. Substituting (6) into (3) and solving, we obtain the solution

$$\hat{n}_{wm}^{VS}(t,r) = \frac{1}{\lambda_{cf}(r)\mathcal{Y}} \left[1 - e^{-\lambda_{ef}(r)t}\right],\tag{7}$$

where the effective reduced exponential rate (due to recycling) is given by

$$\lambda_{ef}(r) = \frac{Q_{nr} + Q_r \eta_f(r)}{\mathscr{V}} + \frac{V_s(r)}{H} + \lambda_{dep}(r) + \lambda_{da}. \tag{8}$$

The first exponential rate can also be written in terms of ACH by defining $ACH_{nr}/3600 = Q_{nr}/\Psi$, $ACH_r/3600 = Q_r/\Psi$, and $ACH_{ef} = ACH_{nr} + ACH_r\eta_f(r)$, where air exchange is divided into a recycled part (ACH_r) and a non-recycled part (ACH_{nr}) . The combined effect of recycling and filtration is measured in terms of the ratio

$$\eta_{ef} = \frac{\text{ACH}_{ef}}{\text{ACH}} = 1 - \frac{\text{ACH}_r}{\text{ACH}} (1 - \eta_f). \tag{9}$$

For $\eta_{ef}=1$, 100% effectiveness is achieved with either no-recycling or perfect filtration. This corresponds to zero influx of the droplet nuclei through the inlet ports. On the other hand, $\eta_{ef}=0$ corresponds to a

totally ineffective filtration system that does not remove any of the droplet nuclei. The other exponential rates in the above equation are taken to remain unaffected by recycling and filtration.

A. Departure from the well-mixed model

The strength of the well-mixed theory is in the simplicity of its prediction and how the effects of recycling and filtration can be accounted for without much difficulty. Its simplicity arises from the fact that the droplet nuclei injected into the room, irrespective of whether they are ejected directly from the infected person or as part of the recycled air through the inlet ports, instantly mix within the room. Neither the location of the infected person nor the location of the inlet port matters, and as a result, $\lambda_{ef}(r)$ accounts for the net removal of nuclei of size r. Furthermore, the room-averaged well-mixed concentration of nuclei is equally available to any receiving host present in the room.

As we will see below, this simplified viewpoint is not applicable when we decide to go beyond the well-mixed assumption and consider specific locations of the source and the sink within the room. The loss of simplicity is due to the fact that for a specific sink location, its distance (relative location) from both the source and the ventilation inlet ports may matter. The probability of finding a nuclei originating from the source and arriving at the sink cannot be treated to be the same as the probability of finding a nuclei originating at the inlet port and arriving at the sink. Again we consider the three different scenarios discussed in the context of the well-mixed theory, now in the context of departure from the well-mixed theory.

Pathogen influx from an infected individual: In the scenario where the infected person is the only source (i.e., $n_S = 0$), let us now consider the normalized concentration of nuclei of size r at a fixed sink location \mathbf{x}_{si} as a function of time after the arrival of an infected person (source) at location \mathbf{x}_{so} . The normalized concentration can be denoted as $\hat{n}^V(t,\mathbf{x}_{si},\mathbf{x}_{so},r)$, which corresponds to the normalized concentration of nuclei of size r at the sink location, t seconds after the arrival of the source to the source location. The normalization is achieved by dividing the unnormalized droplet nuclei concentration by the source ejection rate $Q_b n_V(r)$, and as a result, the normalized concentration can be interpreted as the nuclei concentration at the sink location for a unit ejection rate by the source.

We expect $\hat{n}^V(t, \mathbf{x}_{si}, \mathbf{x}_{so}, r)$ to remain zero for $t < t_{lag,0}$, where $t_{lag,0}$ is the minimum time it takes for nuclei of size r to travel from the source to the sink. After this initial delay time, $\hat{n}^V(t, \mathbf{x}_{si}, \mathbf{x}_{so}, r)$ will increase steadily and approach a steady asymptotic value. In a particular instance (or realization) of a source and sink located somewhere within the room, the normalized concentration will be a stochastic quantity. In other words, although the general trend of the normalized concentration being zero for some delay time and then increasing toward an asymptotic value will hold, there will be fluctuations about this general trend due to the turbulent nature of the flow. Here, we interpret $\hat{n}^V(t, \mathbf{x}_{si}, \mathbf{x}_{so}, r)$ as an ensemble average taken over an ensemble of realizations, which explains the smooth behavior. A schematic of $\hat{n}^V(t, \mathbf{x}_{si}, \mathbf{x}_{so}, r)$ (solid red line), along with the corresponding schematic of a particular realization (solid blue line), is shown in Fig. 1(d).

The double average $\hat{n}^V(t, \mathbf{x}_{si}, \mathbf{x}_{so}, r)$ over all possible source and sink locations can be formally expressed as

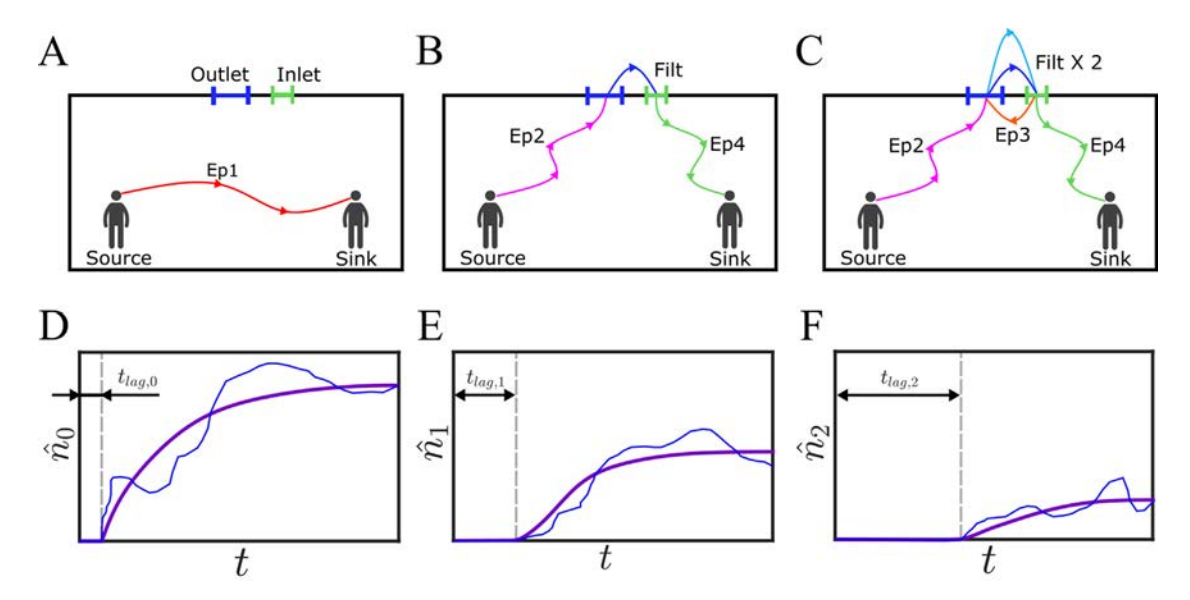


FIG. 1. Schematic of how an ejected pathogen from a source could reach a sink through different routes: (a) direct route (i.e., route Ep1 from the source to the sink without passing through the ventilation system), (b) indirect route with a single pass through the ventilation system [i.e., route (Ep2 + Filt + Ep4) representing the path source—outlet—inlet—sink], and (c) indirect route with two passes through the ventilation system [i.e., route (Ep2 + Filt + Ep3 + Filt + Ep4) representing the path source—outlet—inlet—outlet—inlet—sink]. For each route, a schematic of the normalized pathogen concentration vs time at the sink location is shown in panels (d)—(f) for a particular realization (blue curve) and for the ensemble average (thick purple curve).

$$\langle\langle \hat{n}^V \rangle\rangle(t,r) = \frac{1}{\mathscr{V}^2} \int \int \hat{n}^V(t,\mathbf{x}_{si},\mathbf{x}_{so},r) d\mathbf{x}_{si} d\mathbf{x}_{so}.$$
 (10)

Statistical properties of how the normalized concentration \hat{n}^V deviate from the double average as the source location, sink location, and their distance were varied within the room was considered in detail by Salinas *et al.*²⁴ Their three major conclusions are as follows: (i) $\langle \langle \hat{n}^V \rangle \rangle (t,r)$ is very well approximated by the well-mixed model given in (4); (ii) at source–sink separation distances (i.e., $|\mathbf{x}_{si} - \mathbf{x}_{so}|$) below 5 m, the droplet nuclei concentration is substantially larger than that predicted by the well-mixed model; and (iii) this deviation from the well-mixed theory can be easily accounted for with a correction function that depends on the source–sink separation distance.

Pathogen influx from inlet ports: In the scenario where the influx is only through the inlet ports (i.e., $Q_b=0$), we consider the normalized concentration of nuclei of size r at a fixed sink location \mathbf{x}_{si} as a function of time after nuclei injection has been initiated through the inlet ports. The normalized concentration is denoted as $\hat{n}^S(t,\mathbf{x}_{si},r)$ and the normalization is achieved by dividing the unnormalized droplet nuclei concentration by the surface ejection rate $Q \, n_S(r)$. Hence, $\hat{n}^S(t,\mathbf{x}_{si},r)$ can be interpreted as the nuclei concentration at the sink location for a unit surface ejection rate at the inlet ports. The average of $\hat{n}^S(t,\mathbf{x}_{si},r)$ over all possible sink locations can be formally expressed as

$$\langle \hat{n}^S \rangle_{si}(t,r) = \frac{1}{\mathscr{V}} \int \hat{n}^S(t, \mathbf{x}_{si}, r) \, d\mathbf{x}_{si},$$
 (11)

where $\langle \cdot \rangle_{si}$ indicates an average over all sink locations.

The influx is through the inlet ports instead of the infected person, and as a result, $\hat{n}^S(t, \mathbf{x}_{si}, r)$ and its average $\langle \hat{n}^S \rangle_{si}(t, r)$ can be compared against $\hat{n}^V(t, \mathbf{x}_{si}, \mathbf{x}_{so}, r)$ and its double average. In particular, in Sec. IV, we will examine the statistical properties of $\hat{n}^S(t, \mathbf{x}_{si}, r)$

following the approach of Salinas $et~al.^{24}$ The three major questions to be addressed are: (i) is $\langle \hat{n}^S \rangle_{si}(t,r)$ well-approximated by the well-mixed model given in (4)? (ii) What is the level of nuclei concentration variation about the average as the location of the sink is varied over the indoor space? and (iii) If needed, can this deviation from the well-mixed theory be easily accounted for with a correction function?

Pathogen influx both from an infected individual and inlet ports: As the third scenario, we consider pathogen influx both directly from the infected individual (source) and from the inlet air stream. Again, we restrict the influx through the inlet ports to be the result of recycling and imperfect filtration. The normalized concentration can be expressed as an infinite series as

$$\hat{n}^{VS}(t, \mathbf{x}_{si}, \mathbf{x}_{so}, r) = \hat{n}_0(t, \mathbf{x}_{si}, \mathbf{x}_{so}, r) + \hat{n}_1(t, \mathbf{x}_{si}, \mathbf{x}_{so}, r) + \hat{n}_2(t, \mathbf{x}_{si}, \mathbf{x}_{so}, r) + \cdots,$$
(12)

where $\hat{n}_0(t, \mathbf{x}_{si}, \mathbf{x}_{so}, r)$ corresponds to the normalized concentration of nuclei of size r at the sink location t seconds after the arrival of the source to the source location, accounting for only those nuclei that arrive at the sink through the direct route. This *direct route* (or zerothorder route) from the source to the sink is schematically depicted in Fig. 1(a). It can be readily seen that $\hat{n}_0(t, \mathbf{x}_{si}, \mathbf{x}_{so}, r)$ is the same as $\hat{n}^V(t, \mathbf{x}_{si}, \mathbf{x}_{so}, r)$ and, thus, can be interpreted as the time evolution of nuclei concentration (i.e., number of nuclei per unit volume) around the sink for a steady release of one nuclei per second by the source after arrival at t = 0, only due to the direct route of transmission.

In the summation given in (12), $\hat{n}_1(t, \mathbf{x}_{si}, \mathbf{x}_{so}, r)$ corresponds to the normalized concentration of nuclei of size r at the sink location, t seconds after the arrival of the infected individual to the source location, accounting for only those nuclei that arrive at the sink from the source following a single pass through the ventilation system (i.e.,

exiting the room once through the outlet and reentering the room through the inlet without being filtered). This "first-order" route from the source to the sink is schematically depicted in Fig. 1(b). Again, $\hat{n}_1(t, \mathbf{x}_{si}, \mathbf{x}_{so}, r)$ must be interpreted as the time evolution of nuclei concentration for a steady release of one nuclei per second by the source due to the first-order route of arrival. It can be expected that $\hat{n}_1(t, \mathbf{x}_{si}, \mathbf{x}_{so}, r)$ will remain zero for $t < t_{lag,1}$, where the first-order delay $t_{lag,1}$ will be longer than $t_{lag,0}$. After this initial delay time, $\hat{n}_1(t, \mathbf{x}_{si}, \mathbf{x}_{so}, r)$ will increase steadily and approach an asymptote, whose value will be lower than the asymptotic value of $\hat{n}_0(t, \mathbf{x}_{si}, \mathbf{x}_{so}, r)$. A schematic of the ensemble average $\hat{n}_1(t, \mathbf{x}_{si}, \mathbf{x}_{so}, r)$ is shown in Fig. 1(e) as the solid red line. We note that in a particular realization, shown as a blue solid line, there will be chaotic fluctuations about the average.

Similarly, $\hat{n}_2(t, \mathbf{x}_{si}, \mathbf{x}_{so}, r)$ corresponds to the "second-order" route from the source to the sink where the nuclei pass through the ventilation system twice without being filtered [see Fig. 1(c)]. $\hat{n}_2(t, \mathbf{x}_{si}, \mathbf{x}_{so}, r)$ and higher order terms follow the same pattern, with each of their delay time being longer than any previous delay times and each asymptotic value being lower than an earlier value [see Fig. 1(f)]. The sum over the different routes as given in (12) yields the time evolution of the total normalized nuclei concentration. Based on the well-mixed theory, it can be easily argued that the series converges provided at least one of the decay mechanisms presented in (5) is active. In other words, provided at least one of the decay mechanisms (filtration, settling, wall-deposition, or deactivation) is non-zero, the series will converge to yield the finite sum $\hat{n}^{VS}(t, \mathbf{x}_{si}, \mathbf{x}_{so}, r)$.

For sufficiently large-sized nuclei, the decay due to settling and filtration will be sufficiently high that only the first few terms are sufficient. In other words, for such large nuclei, the probability of reentering the room is negligible. On the other hand, for very small nuclei, the probability of reentry may not be negligible. However, the additional time taken by the nuclei for each reentry, along with the deactivation rate, will ensure that the higher order terms contribute progressively less, even in the case of small nuclei.

The double average of $\hat{n}^{VS}(t, \mathbf{x}_{si}, \mathbf{x}_{so}, r)$ over all possible source and sink locations can be expressed as

$$\langle\langle \hat{n}^{VS}\rangle\rangle(t,r) = \frac{1}{\psi^2} \int \int \hat{n}^{VS}(t,\mathbf{x}_{si},\mathbf{x}_{so},r) d\mathbf{x}_{si} d\mathbf{x}_{so}.$$
 (13)

It is of interest to examine how well this double average is approximated by the well-mixed prediction given in (4). The simplicity of the well-mixed assumption is clear. The converged sum of the infinite series is directly obtained without having to book-keep the zeroth-, first-, and higher-order concentrations explicitly. However, if we are interested in specific source–sink combinations, then departure from $\langle \langle \hat{n}^{VS} \rangle \rangle(t,r)$ may be substantial, and one may need to consider the summation in (12) explicitly.

IV. STATISTICS OF NUCLEI ENTERING THROUGH THE INLET

In this section, we will investigate the level of well-mixedness of droplet nuclei that have been injected into the room through the inlet vents. The droplet trajectories obtained from the large eddy simulations are post-processed to obtain statistically converged normalized nuclei concentration \hat{n}^{S} as a function of time, sink location, and droplet size. It is of interest to examine how well the average over all sink

locations [i.e., $\langle \hat{n}^S \rangle_{si}(t,r)$] is approximated by the well-mixed model given in (4). We will check whether the room-averaged concentration of nuclei injected at the inlet ports follow the same pattern as the room-averaged concentration of nuclei ejected by an infected source located within the room.

A. Sink-averaged statistics

Figure 2(a) displays the sink-averaged statistics $\langle \hat{n}^S \rangle_{si}(t,r)$ plotted as a function of t for ten different values of droplet nuclei size r. Since the average nuclei concentrations have been divided by their terminal value, all the curves start from zero and approach the terminal value of unity. Also plotted in the figure are the exponential curve fits, which compare quite well against the LES results. The behavior is very similar to what was presented in Ref. 24. Figure 2(a) is for the case of ACH = 5 with similar results being observed at other values of ACH.

In the inset of Fig. 2(b), we plot the exponential rates λ obtained from the results shown in Fig. 2(a) for ACH = 2.5 and ACH = 5 for varying nuclei sizes parameterized in terms of their settling velocity V_s . Also shown are the corresponding exponential rates obtained from the fits of $\langle \langle \hat{n}^V \rangle \rangle (t,r)$. These results were reported in Ref. 24, and they indicate that the exponential evolution of the double-averaged nuclei concentration closely follows the analytical estimate λ_{wm} given in (5). Figure 2(b) firmly establishes that, in the case of injection of pathogen through the inlet ports, the sink-averaged nuclei concentration closely follows the same evolution as the room average in the case of a source located within the room. Furthermore, both these cases are well predicted by the well-mixed model. Based on the analysis presented in Ref. 24, when properly scaled as

$$\tilde{\lambda} = \frac{3600}{\text{ACH}} \lambda \quad \text{and} \quad \tilde{V}_s = \frac{3600}{\text{ACH}} \frac{V_s}{H},$$
 (14)

the resulting $\tilde{\lambda}$ vs \tilde{V}_s plots for the different ACH collapse into a universal dependence. Here, H represents the room height. This result is shown in the mainframe of Fig. 2(b), where departure from perfect collapse between the room-averaged statistics and the sink-averaged statistics for inlet ejection is observed for the largest droplets of non-dimensional settling velocity $\tilde{V}_s \gtrsim 10$. For such large nuclei, the exponential rate λ measured from the simulation results is higher than that predicted by the well-mixed model. Furthermore, the exponential rate of such droplets injected through the inlet is observed to be larger than that ejected by an infected source. A possible explanation is that the average deposition rate of the large droplets is slightly higher than the theoretical estimate of V_s/H , and this increase is enhanced in the case of injection through the inlet vents, whose inflow is directed downward toward the floor.

Irrespective of whether the nuclei are injected through the inlet ports or ejected by the infected source within the room, a steady state of nuclei concentration is reached when the influx is balanced by a combination of floor and wall deposition, and exit through the outlet. (In the analysis of Fig. 2, viral deactivation has been ignored.) Figure 2(c) shows the fraction of nuclei that exit the room through the outlet $\tilde{\chi}_o$, the floor $\tilde{\chi}_f$, and the walls $\tilde{\chi}_w$ after the steady state has been reached. The results are plotted for ten different nuclei sizes and two different ACH values. Also shown are the corresponding theoretical estimates (cross symbols). Since $\tilde{\chi}_o \approx 1$ for the small nuclei, it is clear that they primarily exit the room through the outlet. A small fraction of about 4% of the small nuclei get deposited on the walls and the ceiling.

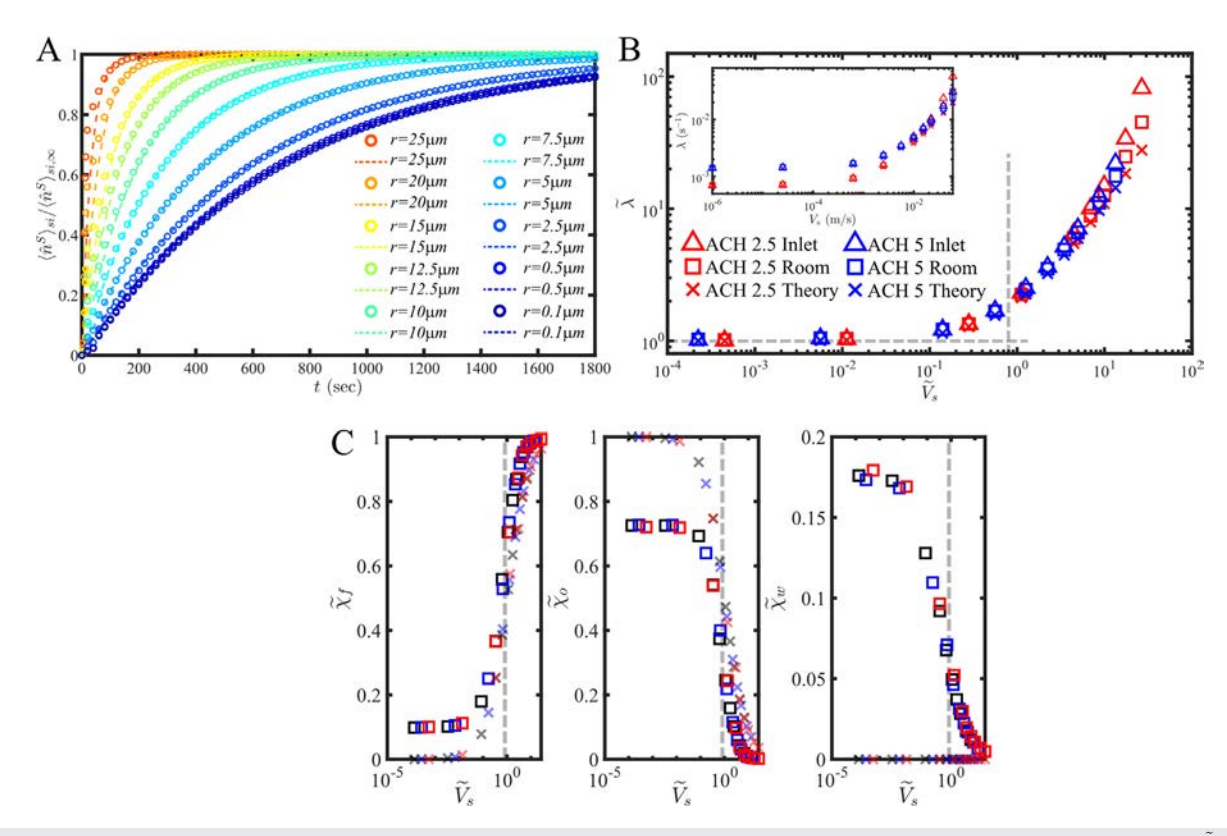


FIG. 2. (a) Decay of nuclei concentration ejected from the inlet vs time. Simulation data "o" vs exponential fit "-" for ACH = 5. (b) ACH-scaled exponential rate $\tilde{\lambda}$ vs ACH-scaled settling velocity \tilde{V}_s for the exponential fits in panel (a). The horizontal dashed line represents $\tilde{\lambda}=1$, which corresponds to the theoretical estimate for very small nuclei. Inset: Dimensional λ vs V_s . (c) Proportion of nuclei that exit through the floor $(\tilde{\chi}_f)$, the outlet $(\tilde{\chi}_o)$, and the walls $(\tilde{\chi}_w)$ relative to the total number of nuclei that were removed. The vertical dashed line represents the cutoff size for airborne nuclei in the well-mixed theory.

As we will see below, this small amount of wall deposition will play an important role when the air is recycled without filtration. On the other hand, as can be expected, the largest droplet nuclei leave the room primarily through gravitational settling onto the floor.

From Fig. 2, we come to the first important conclusion that the room-averaged statistics for nuclei injected either through the inlet or ejected by the infected source are in good agreement with each other and with the well-mixed theory, except for very large nuclei corresponding to a non-dimensional settling velocity of $\tilde{V}_s \gtrsim 10$.

B. Deviation from sink-averaged statistics

We now examine how the normalized nuclei concentration $\hat{n}^S(t,\mathbf{x}_{si},r)$ differs from the average $\langle \hat{n}^S \rangle_{si}(t,r)$ as the sink location is varied within the room for the different nuclei sizes. To illustrate this spatial variation, we focus on the steady state concentration obtained as $t\to\infty$. Figure 3 shows contours of $\hat{n}_\infty^S=\hat{n}^S(t\to\infty)$ for three different nuclei sizes of r=0.1, 5, and 25 μ m, plotted on one vertical and one horizontal plane (the location of the planes are shown in the accompanying isometric view of the room). The corresponding probability density functions (PDFs) of $\hat{n}_\infty^S/\langle \hat{n}^S \rangle_{si,\infty}$ are also presented in the figure. For the smallest nuclei, it can be seen that the concentration is higher in the path of the four inlet jets. This is apparent in both the contour plots on the vertical and the horizontal planes. However, from

the PDF, it is clear that the concentration of the smallest nuclei does not vary much over the entire room as a result of vigorous mixing. This can also be observed in the relatively small value of the standard deviation σ^S for $\tilde{V}_s < 0.4$. In contrast, the concentration of the larger nuclei vary substantially within the room, with the concentration in the path of the inlet jets being more than twice the room average. This large variation in the nuclei concentration can be observed in the rapid increase in the value of standard deviation (σ^S) and skewness (Sk^S) for large values of \tilde{V}_s . Interestingly, the concentration of both the small and large nuclei is slightly higher than the average in the four corners of the room.

These results must be compared against similar statistics presented in Ref. 24 for the scenario where the ejection of droplet nuclei into the room was from an infected individual as opposed to being through the inlet ports. First, we compare the results presented in Fig. 3 against the corresponding plots of $\langle \hat{n}^V \rangle_{so,\infty} / \langle \langle \hat{n}^V \rangle \rangle_{\infty}$ presented in Ref. 24 for varying sink locations $(\langle \cdot \rangle_{so}$ corresponds to an average over all possible source locations within the room). The behavior was qualitatively very similar with small variation in the concentration of small nuclei and progressively larger variation for larger nuclei. An important difference can be noticed. In the case of $\langle \hat{n}^V \rangle_{so,\infty} / \langle \langle \hat{n}^V \rangle \rangle_{\infty}$, the inlet jets are regions of lower-than-average concentration, since there is zero influx of nuclei through the inlet ports, whereas the present

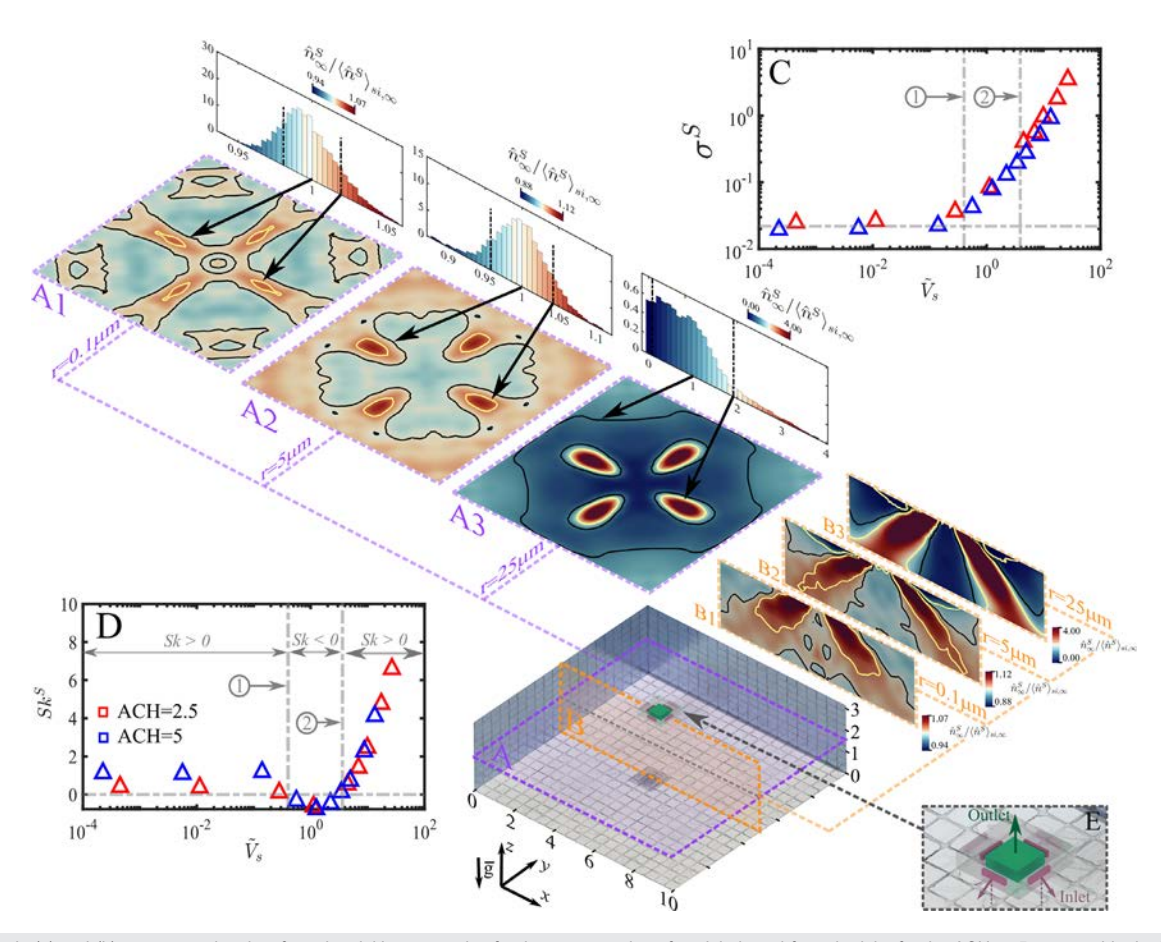


FIG. 3. Panels (a) and (b) are composite plots from the sink's perspective for the concentration of nuclei ejected from the inlet for the ACH = 5 case and in the limit as time tends to infinity. The contour plots are displayed in the horizontal [(a) panels] and vertical [(b) panels] planes shown in the isometric view and labeled A (colored purple) and B (colored orange), respectively. The (A) and (B) planes are at z = 1.6 and y = 5, respectively. Three nuclei sizes are considered, namely, r = 0.1, 5, and 25 μ m, and the probability density function (PDF) is shown above each respective panel. The PDF corresponds to the entire room and not just the selected planes. Furthermore, the insets show the (c) standard deviation σ^S and (d) skewness Sk^S of the PDFs as a function of scaled settling \tilde{V}_s , for all cases. Panel (e) shows an enlarged view of the outlet and inlets.

scenario of injection through the inlet ports complements the injection within the room with higher than average concentration within the inlet iets

A more careful analysis reveals an important difference between the mixing characteristics of nuclei directly from the infected individual and indirectly through the inlet jets. In the case of ejection by an infected source, Salinas *et al.*²⁴ observed that the normalized concentration of even the smallest nuclei can be as large as two to three times the room average, provided the source-to-sink distance is 2 m or smaller. This increase in concentration at shorter separations is balanced by substantially lower-than-average concentrations at source-to-sink distances larger than 7 m.

This trend is not observed in the case of injection through the inlet ports. As discussed above, for the smallest nuclei, except for regions very close to the inlet ports, the nuclei concentration appears far more well mixed. For the ACH = 5 case considered, and for nuclei of size less than 5 μ m, the local concentration seldom deviates by more than 10% from the room average. In stark contrast to the scenario of ejection from an infected source, being close-to or far-away from the

inlet ports does not seem to matter. The excellent mixing of the small nuclei is perhaps due to the substantially higher intensity of the inlet jets, which promote rapid mixing. In contrast, in the case of ejection by an infected source, due to the much lower local flow velocity and less vigorous mixing, it matters far more whether the receiving host is close-by or far-away. We therefore come to the important conclusion that droplet nuclei injected through the inlet ports are far more well-mixed than those ejected by an infected source located within the room, and this difference is due to the substantially higher intensity of the inlet jets. This observation will be further strengthened in Secs. V and VI with additional statistical results.

V. STATISTICAL FRAMEWORK FOR RECYCLING AND FILTRATION

We begin this section by noting that the effects of recycling and filtration are easily incorporated in the well-mixed model as given in (7). Thus, the focus here is to establish the departure from the well-mixed model and develop a simple correction function as was done in Ref. 24. This will be accomplished with the use of the LES results.

The straightforward approach to incorporating recycling and filtration in the LES simulations is to keep track of the droplet nuclei that exit the room through the outlet and probabilistically reintroduce some of them back into the room according to the filtration efficiency of the air-handling system. Such an approach will require performing numerous LES for each specific combination of sourcesink locations within the room, and for each values of ACH and filtration efficiency. Thus, a straightforward approach is computationally expensive. The approach to be followed here combines the results of the source-to-sink direct route investigated by Salinas *et al.*²⁴ with the inlet-to-sink results presented in Sec. IV to obtain a general description that is applicable for all values of recycling and filtration.

This is accomplished by considering the following four elementary statistics: (Ep1) statistics of nuclei traveling directly from the source to the sink, (Ep2) statistics of nuclei traveling from the source to the outlet, (Ep3) statistics of nuclei traveling from the inlet to the outlet (i.e., from the inlet ports to the outlet port), and (Ep4) statistics of nuclei traveling from the inlet to the sink. We recall that all four EPs have already been studied and well understood. The statistics of source-to-sink and source-to-outlet have been reported in Ref. 24, while the statistics of inlet-to-sink and inlet-to-outlet have been discussed in Sec. IV. With the aforementioned elementary processes, we can construct the zeroth-, first-, and higher-order routes shown in Fig. 1 according to the following sequential superposition

$$zeroth\text{-}order = Ep1, \\ first\text{-}order = Ep2 + Filt + Ep4, \\ second\text{-}order = Ep2 + Filt + EP3 + Filt + Ep4, \\ higher\text{-}order = \\ \end{cases}$$
 (15)

From Fig. 1(b), we note that the first-order route of nuclei from the source to the sink can be traced as source-to-outlet (Ep2), followed by recycling and filtration within the ventilation system (Filt), and followed by the inlet-to-sink trajectory (Ep4). Similar interpretations can be given to the second and higher-order routes. In the above, the process denoted as "Filt" accounts for the filtration of nuclei that pass through the air conditioning unit. Note that while Filt accounts for the details of the filtration efficiency of the air filter, the other four processes are independent of the filtration details. Thus, the strategy is to use the pre-computed statistics of the four elementary processes and compute the results of the different routes as given above, for any filtration efficiency through post-processing. Once the zeroth-, first-, and higher-order routes are obtained, they can be summed up as given in (12) to obtain the overall nuclei concentration at any sink location.

Statistics of the zeroth-order route: The statistics of the direct route from the source to the sink has already been addressed in Ref. 24. This is the only route of pathogen arriving at the sink in the case of perfect filtration or no recycling (i.e., all other routes are zero in this case). We define

$$f_0(\tau, \mathbf{x}_{si}, \mathbf{x}_{so}, r) \tag{16}$$

as the fraction of droplets that were at the source and were later observed at the sink after a time interval of τ . From this, the requisite normalized nuclei concentration can be evaluated as

$$\hat{n}_0(t, \mathbf{x}_{si}, \mathbf{x}_{so}, r) = \frac{1}{\mathscr{V}_{si}} \int_0^t f_0(\tau, \mathbf{x}_{si}, \mathbf{x}_{so}, r) \, d\tau, \tag{17}$$

where \mathcal{V}_{si} represents the sink volume. While $\hat{n}_0(t, \mathbf{x}_{si}, \mathbf{x}_{so}, r)$ represents a response to a steep change (i.e., a response to a steady ejection at the source starting at t = 0), $f_0(\tau, \mathbf{x}_{si}, \mathbf{x}_{so}, r)$ represents a response to a delta change (i.e., a response to an instantaneous ejection at the source at t = 0). This interpretation explains the integral relation given in (17).

Statistics of the first-order route: From Fig. 1(b) and from (15), we recognize that two elementary statistics are needed to consider the first-order indirect route. We first define

$$f_{so-ou}(\tau, \mathbf{x}_{so}, r)$$
 and $f_{in-si}(\tau, \mathbf{x}_{si}, r)$ (18)

as the fraction of nuclei of size r, which were at the source and were later observed to exit the room through the outlet after a time interval of τ and as the fraction of droplets that entered the domain through the inlet ports and were later observed at the sink location after a time interval of τ , respectively. Both these functions can be obtained by post-processing the simulation results.

We proceed to calculate the fraction of nuclei that were at the source and later observed at the sink after a time interval of τ , not directly, but after passing through the ventilation system once. From Fig. 1(b), we identify that this process requires the nuclei to travel from the source to the outlet, filter through the ventilation system, and finally travel from the inlet to the sink. Based on this, we obtain

$$f_1(\tau, \mathbf{x}_{si}, \mathbf{x}_{so}, r) = \int_0^{\tau - \tau_f} f_{so-ou}(\tau_1, \mathbf{x}_{so}, r) \left(1 - \eta_{ef}(r)\right) \times f_{in-si}(\tau - \tau_f - \tau_1, \mathbf{x}_{si}, r) d\tau_1,$$
(19)

where it is assumed that the recycled air leaving the room through the outlet port takes τ_f duration to reenter the room. In (19), we have imposed the condition that the time it takes to travel from the source to the outlet (i.e., τ_1), the time it takes to recycle through the ventilation system, and the time it takes to travel from the inlet to the sink must add up to τ . The integral accounts for all possible values of τ_1 . The above expression can be rewritten as

$$f_1(\tau) = (1 - \eta_{ef})\tilde{f}_1(\tau - \tau_f),$$

where

$$\tilde{f}_1(\xi) = \int_0^{\xi} f_{so-ou}(\tau_1) f_{in-si}(\xi - \tau_1) d\tau_1.$$
 (20)

The advantage is that since f_{so-ou} and f_{in-si} are independent of the filtration details, the integral \tilde{f}_1 can be pre-computed. f_1 can then be calculated for any value of η_{ef} and τ_f . From this, the first-order normalized nuclei concentration can be evaluated as

$$\hat{n}_1(t, \mathbf{x}_{si}, \mathbf{x}_{so}, r) = \frac{1 - \eta_{ef}(r)}{\mathscr{V}_{si}} \int_0^t \tilde{f}_1(\tau - \tau_f, \mathbf{x}_{si}, \mathbf{x}_{so}, r) d\tau.$$
 (21)

It can be expected that τ_f is typically small, and for $\tau \gg \tau_f$, the time the recycled air spends within the ventilation system can be neglected, which will simplify the above integral.

Statistics of higher-order routes: The above steps can be followed to construct the normalized nuclei concentration of the higher-order routes. From Fig. 1(c) and from (15), we recognize one additional

elementary statistics is needed to consider the higher-order indirect routes. The inlet-to-outlet transport process (Ep3) is defined by the statistics $f_{ou-in}(\tau,r)$, which represents the fraction of nuclei of size r which were injected with the inlet air stream and were later observed to exit the room through the outlet after a time interval of τ . Note that this statistics is independent of the source and sink locations and can be easily calculated by post-processing the nuclei trajectories in a manner similar to the other statistical quantities.

The fraction of nuclei that were at the source and later observed at the sink after a time interval of τ , having also passed twice through the air conditioning unit can be evaluated as

$$f_{2}(\tau) = \int_{0}^{\tau-2\tau_{f}\tau-2\tau_{f}-\tau_{2}} \int_{0}^{\tau-2\tau_{f}\tau-2\tau_{f}-\tau_{2}} f_{so-ou}(\tau_{1}) (1 - \eta_{ef})^{2} f_{in-ou}(\tau_{2})$$

$$\times f_{in-si}(\tau - 2\tau_{f} - \tau_{1} - \tau_{2}) d\tau_{1} d\tau_{2}, \qquad (22)$$

where the dependence on source/sink locations and r is suppressed. It is again assumed that the recycled air leaving the room through the outlet port takes τ_f duration to reenter the room during each pass. In the above integral, τ_1 represents the time it takes for the nuclei to travel from the source to the outlet, and τ_2 represents the time it takes from the inlet to the outlet. Here, we have imposed the condition that the time it takes to travel from the inlet to the sink must be such that the overall time adds up to τ . The integral accounts for all possible values of τ_1 and τ_2 . The above double integral can be simplified to a single integral with the following manipulation to obtain

$$f_2(\tau) = (1 - \eta_{ef})^2 \tilde{f}_2(\tau - 2\tau_f),$$

where

$$\tilde{f}_{2}(\xi) = \int_{0}^{\xi} f_{in-ou}(\tau_{2}) \tilde{f}_{1}(\xi - \tau_{2}) d\tau_{2}, \tag{23}$$

where the term f_1 has been defined earlier in (20). The interpretation is simple. The function \tilde{f}_1 accounts for source-to-outlet and inlet-to-sink paths. The added effect of the additional path from inlet-to-outlet in the second-order route is included in the definition of \tilde{f}_2 with the integral given in (23).

This procedure can be easily extended to calculate higher-order routes as well. The fraction of nuclei that were at the source and later observed at the sink after a time interval of τ , after passing q-times through the ventilation system can be evaluated as

$$f_q(\tau) = (1 - \eta_{ef})^q \tilde{f}_q(\tau - q \tau_f),$$

where

$$\tilde{f}_{q}(\xi) = \int_{0}^{\xi} f_{in-ou}(\tau_{q})\tilde{f}_{q-1}(\xi - \tau_{q})d\tau_{q}, \tag{24}$$

where it is recognized that the difference between qth and (q-1)th-order route is just an additional passage from the inlet to the outlet and through the filter. This leads to the recursive evaluation of $\tilde{f}_q(\xi)$ in terms of $\tilde{f}_{q-1}(\xi)$. The qth-order normalized nuclei concentration can then be evaluated as

$$\hat{n}_q(t, \mathbf{x}_{si}, \mathbf{x}_{so}, r) = \frac{(1 - \eta_{ef})^q}{\mathscr{V}_{si}} \int_0^t \tilde{f}_q(\tau - q \, \tau_f, \mathbf{x}_{si}, \mathbf{x}_{so}, r) \, d\tau. \tag{25}$$

The hierarchy of routes can then be summed as given in (12) to obtain the net normalized nuclei concentration at the sink.

VI. RESULTS ON ZEROTH-, FIRST-, AND HIGHER-ORDER ROUTES

We calculate the zeroth-, first-, second-, and higher-order normalized nuclei concentrations using the statistical formulation of Sec. V. To isolate the effect of filtration parameters, we will assume $\tau_f=0$, since the time spent in the air-conditioning unit is expected to be small. Figure 4 shows the time evolution of $\langle\langle\hat{n}_q\rangle\rangle$ for $q=0,1,2,\ldots,5$ for three different nuclei sizes of r=0.1,7.5, and 25 μ m, which are shown in frames A, B, and C. While the red lines in the schematics shown in Fig. 1 depict the ensemble average of the time evolution of \hat{n}_q for a particular combination of the source and sink locations, the plots presented in Fig. 4 are averaged over all possible combinations of the source and sink locations within the room and thus present a room-averaged picture.

For all nuclei sizes, the plots of $\langle\langle\hat{n}_0\rangle\rangle$ as a function of time (black solid line) are the same as those obtained in Ref. 24, and they correspond to nuclei concentration in the limit of perfect filtration with no nuclei reentering the room. Note that $\langle \langle \hat{n}_0 \rangle \rangle$ represents the direct route and, therefore, is not affected by $\eta_{\it ef}$. The higher-order normalized concentrations $\langle\langle \hat{n}_1 \rangle\rangle$, $\langle\langle \hat{n}_2 \rangle\rangle$, etc. depend on the effective filtration efficiency $\eta_{\it ef}$. In Fig. 4, these higher-order concentrations are plotted for $\eta_{ef} = 0$ as blue, red, and other dashed lines. We observe $\langle \langle \hat{n}_1 \rangle \rangle$ to be smaller than $\langle \langle \hat{n}_0 \rangle \rangle$, $\langle \langle \hat{n}_2 \rangle \rangle$ to be smaller than $\langle \langle \hat{n}_1 \rangle \rangle$, and so on. Two factors contribute to this reduction. First, on average, it takes progressively more time for the nuclei to travel from the source to the sink in each higher-order route compared to the lower-order route. Second, due to floor sedimentation and wall deposition, at each order, the rate at which nuclei enter the room is higher than the rate at which they exit through the outlet. In particular, with increasing V_s , the loss of nuclei to sedimentation on the floor is substantial and contribute to a rapid reduction in the higher-order contributions.

The case of $\eta_{ef}=0$ is a limiting case where all the nuclei that leave the room reenter through the inlet. In reality, even in the absence of a filter, it can be expected that some of the droplet nuclei will be lost within the ventilation system and as a result, typically, $\eta_{ef}>0$ for all nuclei sizes.

Nevertheless, in the limit $\eta_{ef} = 0$, the loss of nuclei is only through wall and floor deposition, and we have

$$\langle \langle \hat{n}^{VS} \rangle \rangle (t,r) = \langle \langle \hat{n}_0 \rangle \rangle (t,r) + \langle \langle \hat{n}_1 \rangle \rangle (t,r) + \cdots, \tag{26}$$

which in frames D, E, and F correspond to the sum of the dashed lines with the black solid line. The resulting normalized nuclei concentration is well-approximated by the well-mixed model given in (7) with the exponential rate given by

when
$$\eta_{ef} = 0$$
: $\lambda_{ef}(r) = \frac{V_s(r)}{H} + \lambda_{dep}(r) + \lambda_{da}$. (27)

This result is also shown in frames D, E, and F as the solid red line. Thus, while the black solid line corresponds to perfect filtration $(\eta_{ef} = 1)$, the red solid line corresponds to the other limit where

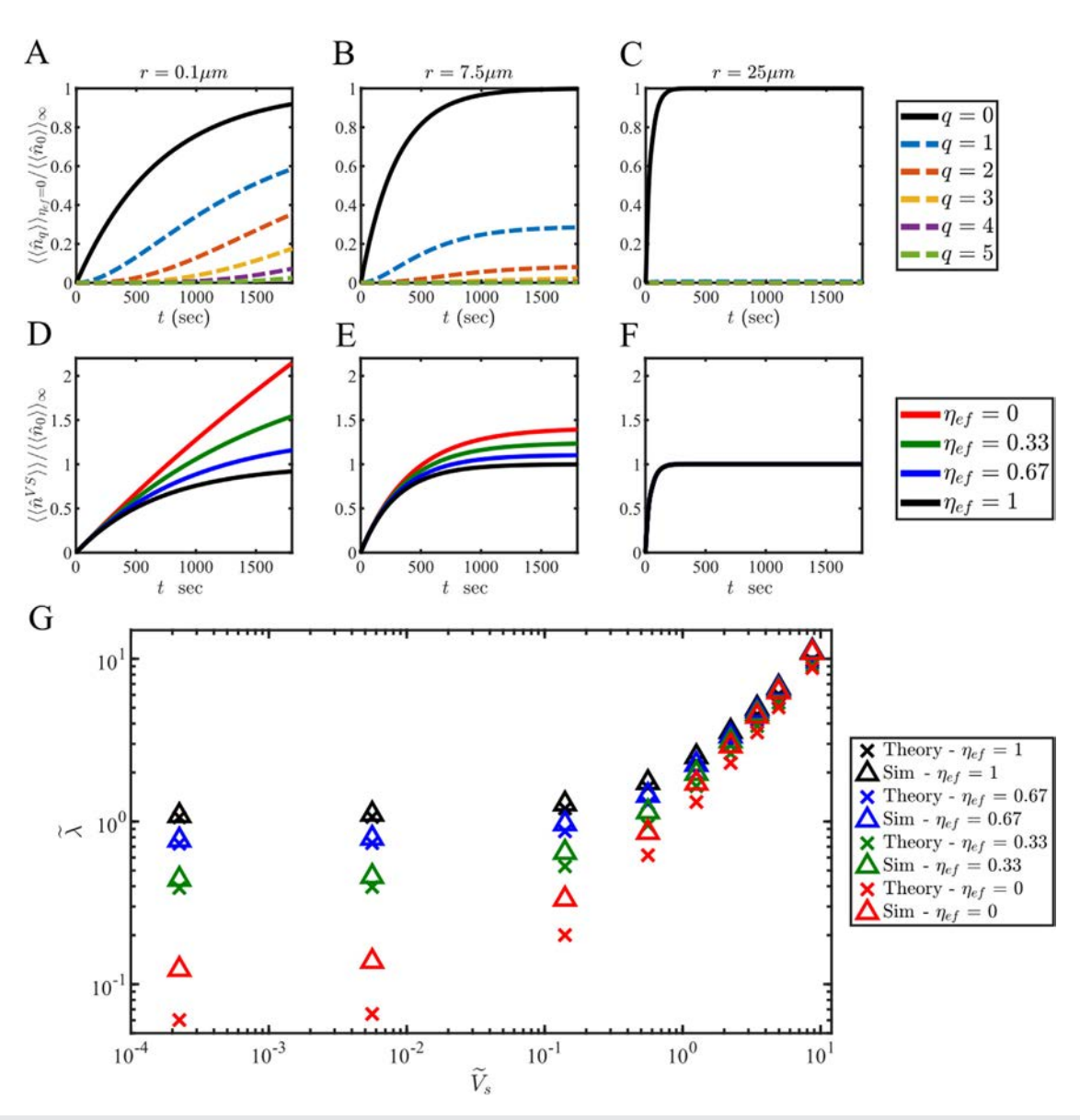


FIG. 4. Time evolution of the normalized room-averaged nuclei concentration subject to four different filtration efficiencies in response to a unit step function ejection for three nuclei sizes (a) r=0.1, (b) r=7.5, and (c) $r=25\,\mu\text{m}$. Time evolution of the normalized proportion of the room-averaged concentration that resulted from nuclei that reentered the room through the inlet q times for (d) r=0.1, (e) r=7.5, and (f) $r=25\,\mu\text{m}$. (g) Dimensionless exponential rate $\tilde{\lambda}$ vs dimensionless settling velocity \tilde{V}_s for the room-averaged concentration with different filtration efficiencies compared to the well-mixed model (cross symbols). Viral deactivation is taken into account with $\lambda_{da}=8.33\times10^{-5}\,\text{s}^{-1}$.

virus-laden nuclei reenter the room ($\eta_{ef}=0$) without any loss. The difference between the two is large in the limit of small nuclei. However, for large nuclei that do not easily exit the room through the outlet stream, the difference is small. Also shown in the figure are plots of $\langle \langle \hat{n}^{VS} \rangle \rangle (t,r)$ at $\eta_{ef}=0.66$ and 0.33. Since $\langle \langle \hat{n}_{q}^{S} \rangle \rangle$ are multiplied by $(1-\eta_{ef})^q$, contributions from higher-order routes are substantially reduced when filtration efficiency η_{ef} increases.

An important effect of recycling without proper filtration becomes clear for small nuclei. For a typical ACH value of O(1) in a residential or office setting, nuclei of radius 2.5 μ m and smaller reach their terminal concentration within about a half hour (\approx 1800 s) after the arrival of the infected person into the room in the case of perfect filtration ($\eta_{ef}=1$). In contrast, when nuclei are allowed to reenter the room without filtration, the concentration of smaller nuclei continues to build up for hours to reach substantially higher values. Efficiency of recycling and filtration (i.e., η_{ef}) is an important parameter for all sizes except those larger than 20 μ m in radius. The above-mentioned 20 μ m size corresponds to an ACH of 5, which results in a non-dimensional

settling velocity of $\tilde{V}_s \approx 10$. As such, at different ACH values, the above-mentioned dimensional size of 20 μ m threshold would vary but would still correspond to a nuclei size with $\tilde{V}_s = 10$.

Figure 4(g) shows the exponential rate λ_{ef} calculated from the time evolution of $\langle\langle \hat{n}^{VS} \rangle\rangle$, for the varying nuclei sizes for the four different values of $\eta_{ef}=1,\,0.66,\,0.33,\,$ and 0. The results obtained from the LES simulations are shown as the triangle symbol. The corresponding well-mixed model predictions, presented as cross symbols, are computed using (8), ignoring the effect of wall deposition (i.e., with $\lambda_{dep}=0$) for lack of a deposition model.

While the results shown in frames A, B, and C do not account for viral deactivation, in frame G, we present the results with the addition of $\lambda_{da}=8.33\times 10^{-5}~{\rm s}^{-1}.^{23}$ In the case of the smallest nuclei, the settling rate is quite small, and its contribution to λ is only about $3\times 10^{-7}~{\rm s}^{-1}$. In the case of $\eta_{ef}=0$, since the room outlet does not contribute to nuclei removal, λ is almost entirely from deactivation. The simulation result includes the effect of wall deposition and, therefore, estimates a value of λ that is substantially larger than the well-mixed model prediction that excludes the effect of wall deposition. It is interesting to note that the loss of droplet nuclei by wall deposition is generally small and can be ignored compared to the loss through outlet and settling. However, in the extreme case of recycling without any filtration, for the small nuclei, loss by outlet and settling become negligible. In this case, wall deposition becomes an important mechanism by which nuclei are removed from the room, without which, the well-mixed concentration will not be accurately predicted.

A. Well-mixedness of first- and higher-order routes

It was shown in Salinas et al.²⁴ that the direct zeroth-order route for specific source-to-sink distances has substantial deviation in normalized nuclei concentration from the room-averaged, well-mixed value. Nuclei concentration at sink locations that are separated from the source by only 2 m or less were on average about two times higher compared to the concentration estimated using the well-mixed model. Correspondingly, at larger source-to-sink separation distances, the nuclei concentration was substantially lower than the well-mixed value. As a result, a correction function was introduced to account for the effect of the source-to-sink distance. It is of interest to evaluate if a similar variation in nuclei concentration exists for the first- and higher-order routes as well, which will be the focus of this subsection.

For the *q*-order route, we calculate the ratio

$$\mathcal{N}_{d,q}(t,r) = \frac{\langle \hat{n}_q \rangle_d(t,r)}{\langle \langle \hat{n}_q \rangle \rangle(t,r)},\tag{28}$$

where in the numerator $\langle \cdot \rangle_d$ corresponds to an average over all source and sink locations within the room such that the distance $|\mathbf{x}_{si} - \mathbf{x}_{so}| = d$. Thus, the numerator corresponds to the average normalized nuclei concentration at the sink provided it is at a distance d from the source. The denominator corresponds to a double average over all the source and sink locations within the room. If the numerator was averaged (with appropriate probability weighting) over all values of the separation distance d, then it will be equal to the denominator. Thus, if the ratio remains close to unity for varying values of d, it is a clear indication of the fact that nuclei are well mixed, the concentration is nearly uniform within the room, and the difference between small and large values of d is not substantial. On the

other hand, if the ratio were to be different from unity, especially with the ratio being significantly larger than unity for small d and significantly smaller than unity at larger d, then deviation from well-mixedness cannot be ignored.

Figure 5(a) shows the temporal evolution of $\mathcal{N}_{d,0}$, $\mathcal{N}_{d,1}$, and $\mathcal{N}_{d,2}$, for nuclei sizes of $r = 0.1 \ \mu \text{m}$ and for distances of d = 1, 2, 4, and 8 m. In the case of the zeroth-order route, substantial deviation from the well-mixed state can be seen with the ratio being significantly larger than unity at small distances and smaller than unity at larger distances. In contrast, in the case of first- and second-order routes, where the influx of nuclei is through high-speed inlet jets, the ratios plotted in red and blue colors are nearly the same for all values of d. Figure 5(b) shows the corresponding results for $r = 7.5 \mu m$, and the observation remains the same that the first- and higher-order routes are far more well-mixed. Plotted in frames C and D are $\mathcal{N}_{d,0,\infty}$, $\mathcal{N}_{d,1,\infty}$, and $\mathcal{N}_{d,2,\infty}$ as a function of \tilde{V}_s for d=1 and 8 m, respectively. In the first- and second-order routes for all smaller sizes of $\tilde{V}_s < 1$, the normalized nuclei concentration remains the same as the room average independent of source-sink distance. Some variation is seen for larger nuclei. In contrast, in the case of the zeroth order direct route, nuclei concentration depends on *d* for all sizes.

As the final step in our investigation of well-mixedness, we investigate if there is a preference to locations close to the inlet ports in the case of first-, second-, and higher-order routes. In other words, we ask the following question: when averaged over all possible source locations, is there an enhanced concentration of droplet nuclei close to the inlet ports? This investigation is not needed for the zeroth-order route, since it only involves the direct path from source-to-sink. We now compute the ratio

$$\mathcal{N}_{so,q}(t, \mathbf{x}_{si}, r) = \frac{\langle \hat{n}_q \rangle_{so}(t, \mathbf{x}_{si}, r)}{\langle \langle \hat{n}_q \rangle \rangle(t, r)},$$
(29)

where in the numerator $\langle \hat{n}_q \rangle_{so}$ corresponds to an average over all source locations within the room and, thus, is still a function of the sink location. If the numerator is further averaged over all sink locations, then it will be equal to the denominator. Thus, if the ratio remains close to unity for varying sink locations, it is a clear indication of the fact that nuclei concentration is well-mixed within the room and the difference between the sink being close to the inlets or farther away is not substantial.

Figure 6 shows contour plots of $\mathcal{N}_{so,1}$ and $\mathcal{N}_{so,2}$ plotted on a vertical and a horizontal plane passing through the center of the box for $r=0.1,\,7.5,\,$ and $25~\mu\mathrm{m}$ for $t\to\infty$. A higher-than-average concentration can be observed in the inlet jets. The increase in concentration above the well-mixed double average is, however, not very large for the small nuclei. Correspondingly, nowhere in the room is the concentration of small nuclei much lower than the room average. This behavior is confirmed by the probability distributions shown in the figure (which correspond to the entire room and not just the horizontal plane A shown in purple) as well as the small value of standard deviation for $\tilde{V}_s < 1$. Large-sized nuclei, however, show substantial spatial variation. However, as will be seen below, the well-mixedness of the first- and higher-order routes for smaller nuclei will outweigh the behavior of larger nuclei in the evaluation of overall pathogen cumulative exposure time.

In essence, it can be concluded that while the zeroth-other route to the sink from the source for the small-sized nuclei has substantial

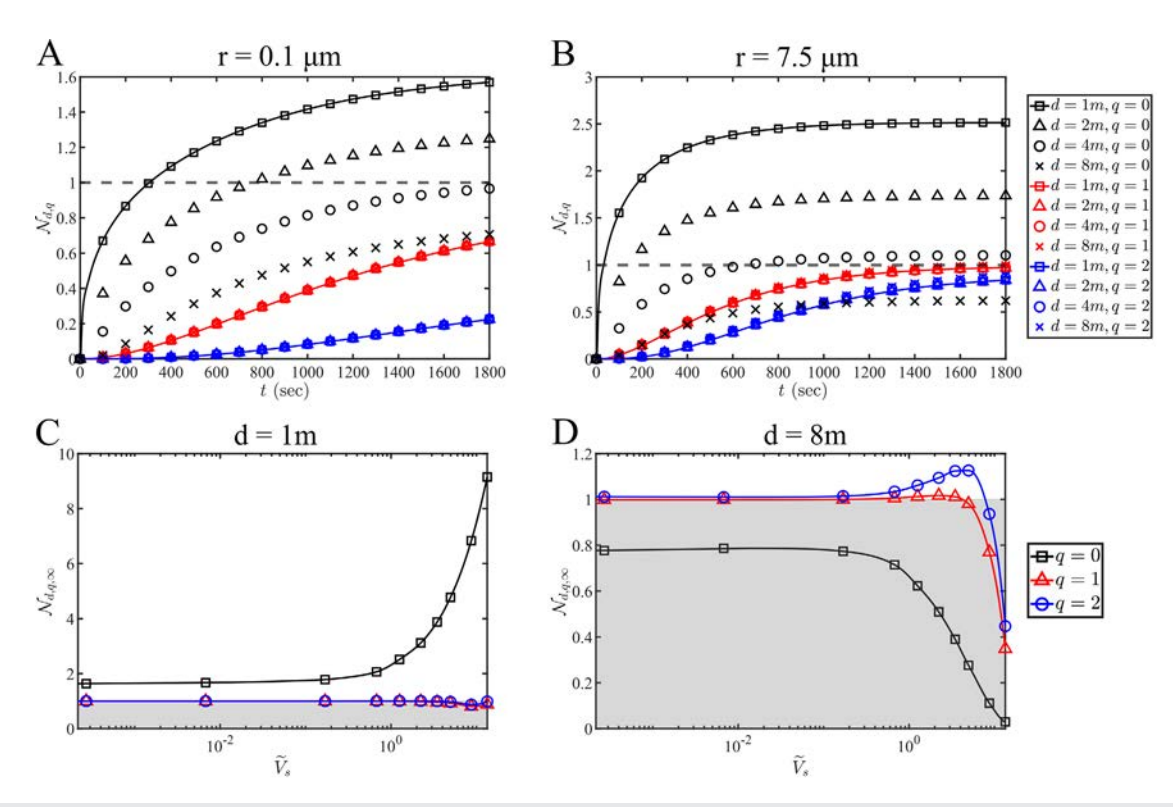


FIG. 5. $\mathcal{N}_{d,q}$ vs time for (a) r=0.1 and (b) $r=7.5~\mu\mathrm{m}$ for ACH =5. Results indicate that for q>0, $\mathcal{N}_{d,q}$ becomes practically independent of d for $r\lesssim7.5~\mu\mathrm{m}$ for ACH $\lesssim5$. Panels (c) and (d) show the steady-state values of $\mathcal{N}_{d,q}$ as a function of the non-dimensional nuclei settling velocity for (c) $d=1~\mathrm{m}$ and (d) $d=8~\mathrm{m}$.

departure from the well-mixed state and shows clear dependence on the source-to-sink separation distance, the higher-order routes that pass through the inlet do not show a large departure from the wellmixed state. As conjectured in Sec. IV, this difference is due to the high-speed mixing induced by the inlet jets compared to the relatively low flow velocity and weaker mixing over the bulk of the room.

VII. CORRECTION FUNCTION WITH RECYCLING AND FILTRATION

Our overarching goal is to enable accurate prediction of cumulative exposure time for any indoor space, given room details, ventilation details (ACH, recycling, and filtration), expiratory ejection details (breathing, speaking, sneezing, etc.), and other details, such as quality of masks. Toward this goal, we adopt the well-mixed model as the baseline, because of its ease of use and ability to account for all physiological, epidemiological, and ventilation details. However, we recognize the need for a correction procedure that will more accurately account for the location of the source and sink within the room, whose important influence was averaged out in the well-mixed model. Such a correction function and its dependence of source-to-sink distance was established in Ref. 24 in the limit of perfect filtration. In this section, we will extend this analysis to systematically include the effect of recycling and filtration. Based on the results of Sec. VI that the virus-laden droplet nuclei injected in the inlet streams are far more well-mixed than those ejected into the room by the infected individual, we expect the correction function to increase with increasing effectiveness of filtration (i.e., for increasing η_{ef}).

Bazant and $Bush^{23}$ presented the following simplified transient well-mixed model of cumulative exposure time (CET):

$$(N\tau)_{wm} = \frac{\epsilon}{Q_h^2 p_m^2 C_q s_r \, \hat{n}_{wm}(\tau)},\tag{30}$$

where the subscript wm indicates estimation using the well-mixed model. In the above, N is the number of receiving hosts in the room, τ is the maximum safe CET for a risk tolerance of ϵ , Q_b is the ejection rate of the infected person and also the inhalation rate of the receiving host, p_m is the filtration efficiency of the mask, which was taken to be a constant and to be the same for both the infected and receiving hosts, C_q is the rate of quanta emitted by the infected person, and s_r is susceptibility or relative transmissibility (see Ref. 23 for details). The overbar accounts for the activity of ejection (breathing, speaking, and singing) by defining the following size-weighted average of the normalized nuclei concentration \hat{n}_{wm}

$$\overline{\hat{n}_{wm}}(\tau) = \frac{\int_0^{r_c} \hat{n}_{wm}(\tau, r) V(r) Q_b n_V(r) dr}{\int_0^{r_c} V(r) Q_b n_V(r) dr},$$
(31)

where $n_V(r)$ is the concentration of exhaled nuclei of radius r that remain airborne, which we take to be given by the experimental measurements of Morawska $et~al.^{45}$ The upper limit of the integrals is taken to be r_c as predicted by the well-mixed theory.²³

As discussed before, there is substantial deviation from well-mixedness in the nuclei concentration. In particular, the normalized

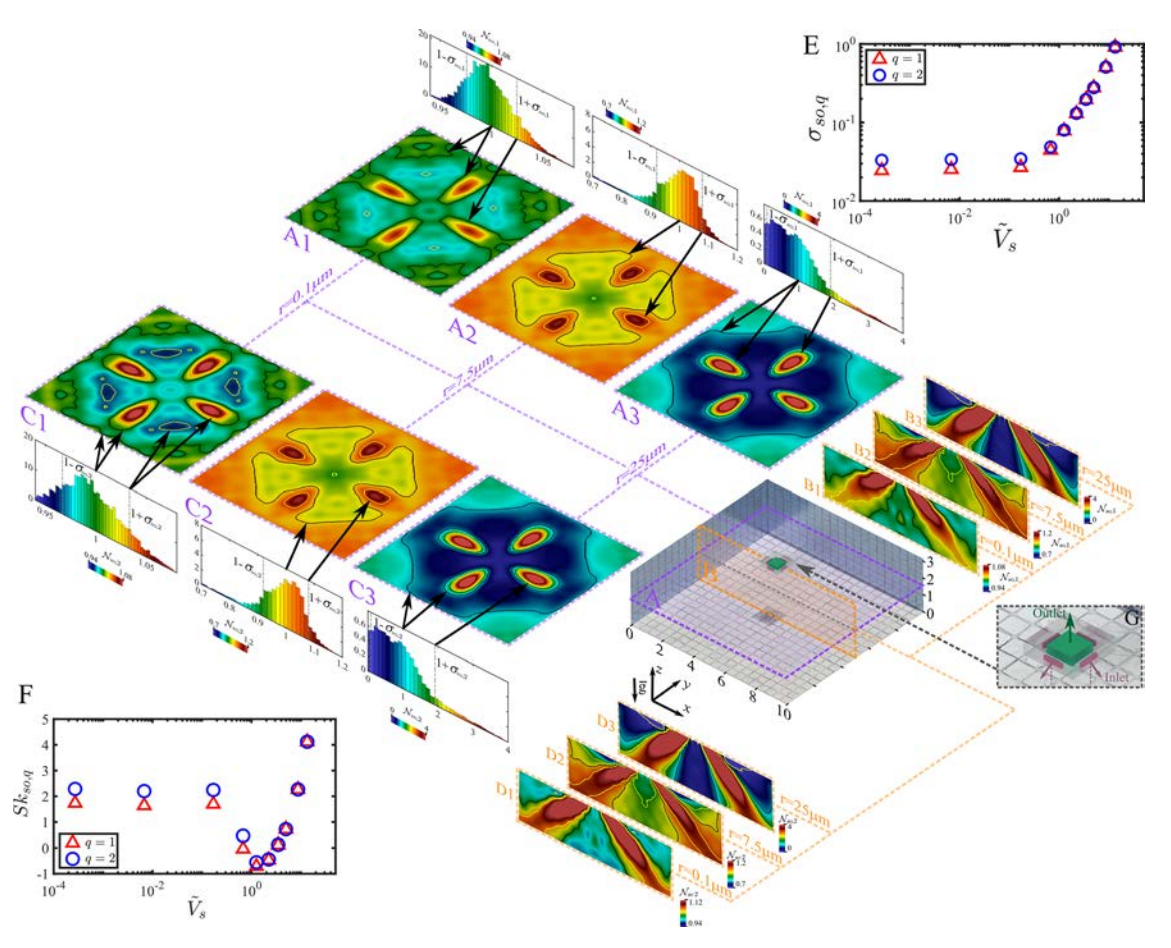


FIG. 6. Contours of $\mathcal{N}_{so,1}$ and $\mathcal{N}_{so,2}$ for three nuclei sizes of r=0.1, 7.5, and 25 μ m in the horizontal plane shown in purple in the isometric view [panels (a) and (c), respectively] and the vertical plane shown in orange [panels (b) and (d), respectively]. See (29) for the definition. Panels (e) and (f) show the standard deviation and skeweness, respectively, vs non-dimensional settling velocity \tilde{V}_s . Panel (g) shows an enlarged view of the outlet and inlets.

nuclei concentration averaged over all source–sink combinations that are a distance d apart, i.e., the sum

$$\langle \hat{n}^{VS} \rangle_d(t,r) = \langle \hat{n}_0 \rangle_d(t,r) + \langle \hat{n}_1 \rangle_d(t,r) + \cdots$$
 (32)

has been observed to vary strongly with d and deviate from the corresponding $\langle\langle \hat{n}^{VS} \rangle\rangle$ that has been double-averaged over all possible source and sink locations (also deviates from the corresponding well-mixed model prediction of \hat{n}_{wm}). As a consequence, a more accurate estimation of CET that accounts for inhomogeneity in the spatial distribution of virus-laden nuclei is given by

$$N\tau = \frac{\epsilon}{Q_b^2 p_m^2 C_q s_r \sqrt{\langle \hat{n}^{VS} \rangle_d}(\tau)},$$

where

$$\overline{\langle \hat{n} \rangle_d}(\tau) = \frac{\int_0^{r_{\text{lim}}} \langle \hat{n}^{VS} \rangle_d(\tau, r) V(r) Q_b n_V(r) dr}{\int_0^{r_{\text{lim}}} V(r) Q_b n_V(r) dr}.$$
(33)

However, $(N\tau)_{wm}$ given in (30) is the well-mixed CET prediction for the entire room, and $(N\tau)$ given in (33) is dependent on the source-sink distance d.

Salinas *et al.*²⁴ reduced the effect of departure from well-mixedness to a single transient *correction function* $\gamma(\tau, d, \eta_{e\!f})$ with the following definition:

$$\gamma(\tau, d, \eta_{ef}) = \frac{(N\tau)_{wm}}{N\tau}.$$
 (34)

The advantage of the above definition of the correction function is that it greatly simplifies the complex manner in which the actual room-scale flow departs from the well-mixed theory into a single function that can be used in conjunction with the well-mixed model.

As per the above transient analysis, the correction function γ is time-dependent. In the steady limit (i.e., as $\tau \to \infty$), the correction will be denoted as γ_∞ , and it is a function of d. The correction function also depends on (i) fluid-mechanical information of the room size, ACH, and η_{ef} , (ii) problem-specific information of where the infected and the receiving hosts are located and the type of mask (N95, surgical, cloth) they are wearing, and (iii) physiological information through

the function $n_V(r)$. Due to the assumption that the viral load and infectivity are independent of nuclei size, γ is independent of these epidemiological factors. It was observed by Salinas $et~al.^{24}$ that the correction function is not strongly dependent on ACH and the nature of ejection activity (breathing, speaking, or sneezing). Therefore, the dominant dependence of γ is only on exposure time τ , source–sink distance d, and η_{ef} .

The normalized nuclei concentration $\langle \hat{n}^{VS} \rangle_d$ averaged over a source–sink distance of d obtained from the ACH = 5 large eddy simulation is averaged as given in (33) with the value $n_V(r)$ taken from Ref. 45 for mouth breathing. The corresponding value of $\hat{n}_{wm}(\tau)$ was also evaluated. With this information, γ was obtained as a function of τ for different values of d=1,2,4, and 8 m. This process was repeated for $\eta_{ef}=1$ corresponding to perfect filtration and $\eta_{ef}=0.66$ and 0.33, and the results are presented in Fig. 7(b). The results for $\eta_{ef}=1$ are the same as those presented in Ref. 24, and the results for imperfect filtration can be seen to somewhat decrease the correction functions.

At shorter distances of d = 1 and 2 m, there is a rapid increase in the correction function reaching peak values of 15 and 4, respectively, at times less than one minute after the arrival of the infected person into the room. As can be expected, at such short times of the order of a few minutes, the correction function is largely unaffected by η_{ef} . This is to be expected since at short times, much of the nuclei concentration at the sink is dominated by the direct route, as it takes a finite time for the nuclei to arrive at the sink through the indirect route of passing through the air handling system. At much larger times, the steadystate value of the correction function (i.e., γ_{∞}) is approached, and this asymptotic value is influenced by recycling and filtration. It is observed that γ_{∞} decreases with decreasing value of η_{ef} . This asymptotic behavior is highlighted in Fig. 7(a). At larger distances, γ displays only a monotonic increase toward the asymptotic value, and the influence of recycling and filtration is lower, which can also be observed in the smaller variation of γ_{∞} for d = 8 in Fig. 7(a).

VIII. DEMONSTRATION AND DISCUSSION

We now have all the information necessary for making comprehensive predictions of CET for scenarios of practical interest. However, prior to making these predictions, we will first quantitatively investigate the effect of filtration at the room averaged level. We consider the two extreme activities of breathing and singing by a sick person located somewhere within the room (exact location does not matter within the well-mixed approximation). We will then monitor the time evolution of pathogen concentration within the room after the arrival of the sick person into the room at t=0. We will then present the result in terms of a size-weighted average normalized nuclei concentration, \hat{n}_{wm} . Following Buonanno *et al.*, ⁶⁰ we define the quanta of inhalation rate at the sink to be given by

$$IR_q = c_v c_i \, \mathcal{V}_h \, \overline{\hat{n}_{wm}} \,, \tag{35}$$

where c_v is the viral load in the sputum measured as RNA copies per mL, c_i is the conversion factor that converts the viral load to infectious quanta, and $\mathcal{V}_h \sim \int_0^{r_{\text{lin}}} V(r)Q_bn_V(r)\,dr$ is the total volume of airborne droplet nuclei ejected expressed in units of ml/h. The quanta of inhalation rate IR_q thus measures the infection quanta per hour that someone in the room will potentially inhale on average, where the infection quanta is defined as the dose of airborne droplet nuclei required to cause infection in 63% of susceptible persons (see Refs. 60 and 61). For fixed values of c_v , c_i , and \mathcal{V}_h , \hat{n}_{wm} is directly proportional to IR_q but focuses only on the room and ventilation characteristics. Thus, plots of \hat{n}_{wm} for different values of η_{ef} allow direct and easy comparison of the effect of recycling and filtration on the quantity of ultimate interest, namely, the quanta of inhalation rate.

Figure 8 shows plots of size-weighted average normalized nuclei concentration, $\overline{\hat{n}_{wm}} = IR_q/(c_c c_i \mathcal{V}_h)$ as a function of time for filtration efficiencies of $\eta_{ef} = 1$, 0.66, 0.33, and 0. These results are obtained from the well-mixed theory presented by Bazant and Bush²³ and take into account the loss of droplet nuclei by exit through the outlet, fall out by gravity, and viral deactivation, but do not account for turbulent wall deposition. The importance of filtration is evident from the picture. Note that size-weighting accounts for the entire range of nuclei sizes ejected by the sick person, which depends on the ejection activity (e.g., breathing and singling). The results for breathing and singing activities are presented, whose airborne nuclei spectra at ejection are taken from Morawska et al. 45 Though the plots of $\overline{\hat{n}_{wm}}$ are close in value for breathing and singing, the value of ejection volume is substantially different with \mathcal{V}_h for singing being 11 times larger than that for breathing, with a corresponding difference in quanta of inhalation rate. The extreme case of zero filtration efficiency results in a quanta of

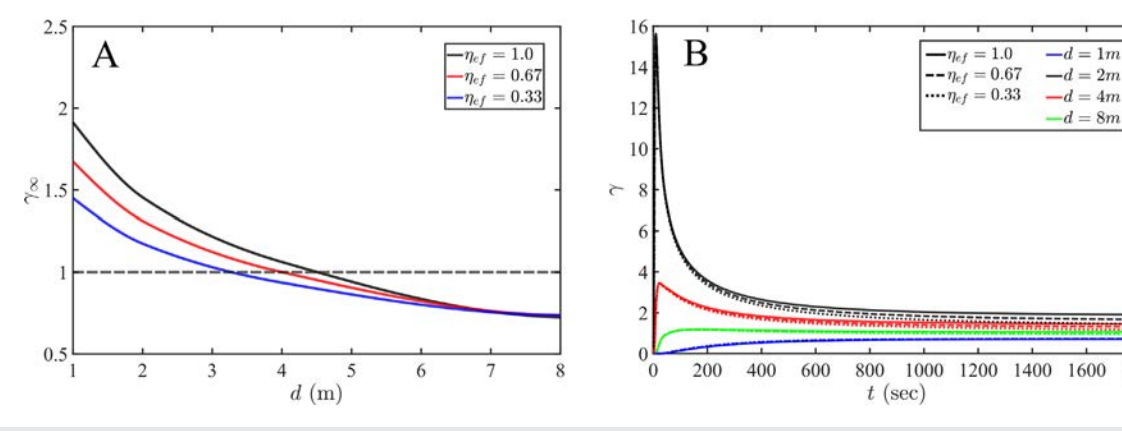
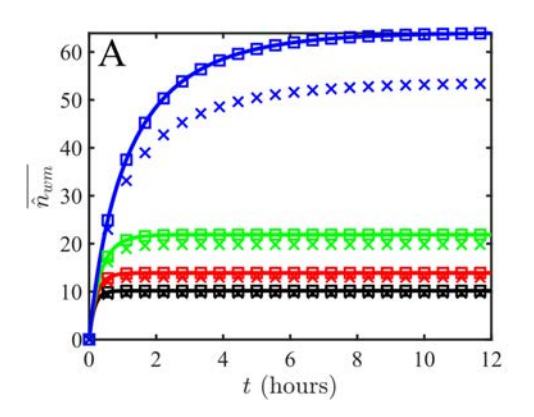


FIG. 7. (a) Steady-state correction function plotted against distance for three filtration efficiencies of 0.33, 0.66, and 1, and (b) time-dependent correction function for the aforementioned filtration efficiencies for source-to-sink distances of 1, 2, 4, and 8 m for ACH = 5.



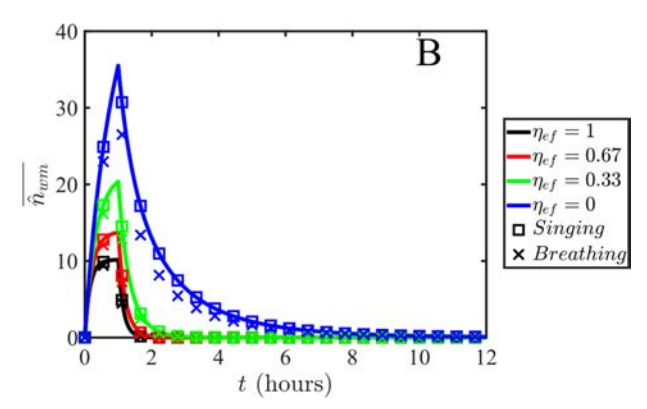


FIG. 8. Size-weighted average normalized nuclei concentration vs time for filtration efficiencies of $\eta_{ef} = 1$, 0.66, 0.33, and 0 from breathing and singing when a sick person occupies the room (a) throughout the period of observation and (b) for a total time of 1 h.

inhalation rate that is 17.6 times larger than the limit of perfect filtration or zero recycling.

It should be immediately cautioned that even when the air conditioning unit recycles the air completely without the addition of any fresh outside air and the recycled air is not filtered, η_{ef} is likely to be non-zero (but small) due to deposition inside the air-handling system and other losses. Furthermore, it can be noted from the figure that for perfect filtration, concentration will reach 95% of its steady-state value after about 35 min. However, for zero filtration (i.e., for $\eta_{ef}=0$), it takes about 10 h for the concentration to reach 95% of the much higher steady-state value. Thus, in the case of $\eta_{ef}=0$, even though the quanta of inhalation rate is 17.6 times larger, it takes many more hours to reach this state.

The results presented in frame A are for the scenario when the sick person stays in the room and serves as a steady source of pathogen for a very long period. Under many scenarios, the source may not remain within the room for such an extended period. Therefore, in frame B, we consider the specific scenario of the source being within the room for only 1 h. In this case, all the plots increase in time for the first hour after the arrival of the source and then decrease with the departure. We observe the concentration of pathogen for $\eta_{ef}=0$ to be 4.6 times larger than that of perfect filtration at the maximal concentration reached after 1 h. In both scenarios, the results for $\eta_{ef}=0.33$ and 0.66 are also plotted. After 1 h, the concentration for $\eta_{ef}=0.33$ and 0.66 are higher by factors of 1.4 and 2.3, respectively. Thus, the effect of filtration remains strong under all scenarios and at all times.

The above predictions are at the level of the well-mixed room average. We now proceed to go beyond the room-averaged prediction of the effects of recycling and filtration by including the source-to-sink distance as an important additional variable with the use of the correction function. This will be demonstrated by revisiting the two examples considered by Bazant and Bush²³ and Salinas *et al.*²⁴ The first is a typical school classroom of area $A = 83.6 \text{ m}^2$ and volume $V = 301 \text{ m}^3$. The second case considered is a nursing home of $A = 22.3 \text{ m}^2$ and $V = 53.5 \text{ m}^3$. Both with a mechanical ventilation of ACH = 8, and we assume speaking to be the mode appropriate for classroom and breathing to be appropriate for the nursing home. Following prior application, in the case of classroom, we assume a transmissibility of 25%, a cloth mask penetration factor of $p_m = 30\%$, and a moderate risk tolerance of $\epsilon = 10\%$. In the case of nursing home, we assume a

transmissibility of 100%, a mask penetration factor of $p_m=10$ %, and a risk tolerance of $\epsilon=1$ %.

In calculating the correction function, we consider the source-sink distance to be the optimal spacing and set $d = \sqrt{A_{floor}/N}$ m, where A_{floor} is the floor area of the room under consideration and N is the total occupancy. In this scenario, we assume that the source and the sink follow this rule and are separated by the optimal spacing permitted by the geometry of the room. Equation (34) is then used to evaluate the corrected safety guideline taking into account the correction factor for the corresponding spacing for different values of occupancy. In both cases, we use the unsteady analysis by accounting for the fact that the correction function is time dependent. The results of the well-mixed model that ignore the source-to-sink separation distance are presented as solid lines for $\eta_{ef} = 1$, 0.67, 0.33, and 0.0 in Fig. 9. Also plotted in the figure as dashed lines are the corresponding results that use the correction function corresponding to the optimal spacing. It should be noted that the correction to the well-mixed model does not depend solely on the separation distance d, but rather on the separation distance scaled by the room size, i.e., $d(A_{floor}H)^{-1/3}$, where the characteristic length of the indoor space is taken as the cubic root of the room volume. This means that for indoor spaces that are very large, such as exhibit halls, the well-mixed model is likely to significantly under-estimate the concentration for separation distances of a few meters, which could correspond to a room-normalized separation distance of a few percent. On the other hand, for small indoor spaces, the well-mixed model may over-estimate the concentration for the same separation distance of a few meters, which could now correspond to a room-normalized separation distance close to 100%. In the examples of Fig. 9, the above discussion is clearly apparent where the correction to the well-mixed model may entail a left-shift or a rightshift to the well-mixed model depending on the scaled separation distance. A left-shift correction indicates that the well-mixed model under-estimates the concentration, whereas a right-shift correction indicates that the well-mixed model over-estimates the concentration. As a result, for a specified exposure time τ , the actual maximum occupancy of a classroom would generally be lower than that predicted by the well-mixed model for the classroom setting. Or when viewed for a fixed occupancy N, the safe exposure time will be generally lower than that predicted by the well-mixed model. On the other hand, for the relatively small nursing home, the safe exposure time τ , or alternatively

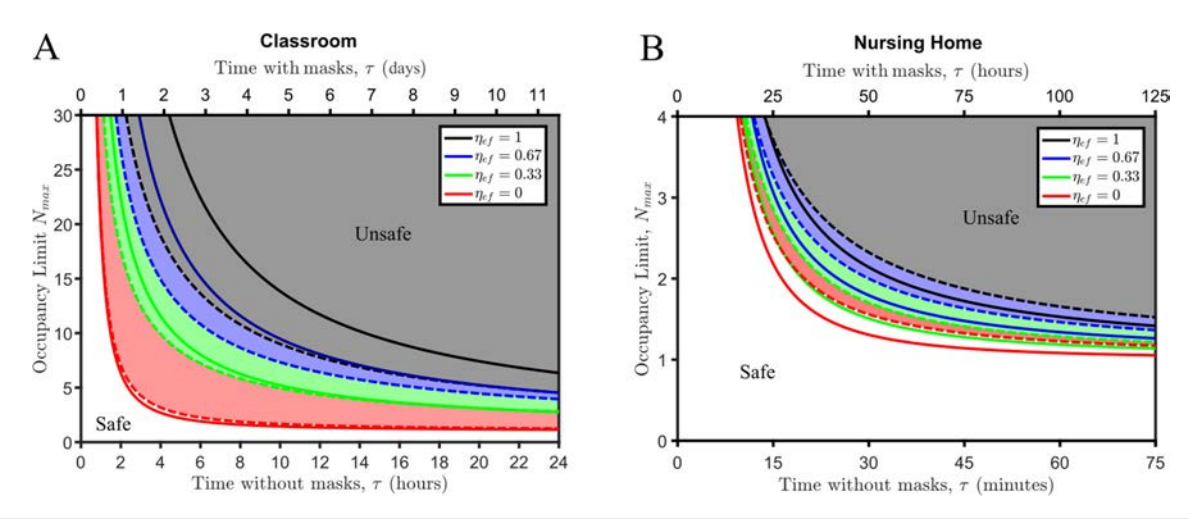


FIG. 9. Occupancy vs cumulative exposure time from well-mixed theory (solid lines) and the correction to the well-mixed theory (dashed lines) taking into account the effect of separation distance for different filter efficiency values η_{ef} for the cases of (a) a classroom and (b) a nursing home.

the actual maximum occupancy *N*, would be generally higher than that predicted by the well-mixed model. The effect of recycling and filtration is also clear. In the nursing home example, for a fixed occupancy of two elderly persons, the safe occupancy time with perfect filtration and without the use of masks is about 35 to 40 min. This safe time decreases to about 20 min when filtration efficiency falls to zero. Similarly, for the classroom example, for a fixed occupancy of 30 students, the safe occupancy time with perfect filtration and without the use of masks is around 3 h, but decreases to about an hour and a half when filtration efficiency falls to zero.

For relatively large indoor spaces, such as in the classroom example, it can be observed that the difference between the well-mixed model prediction and that with the correction function is the largest for $\eta_{ef}=1$. With decreasing η_{ef} , the difference between the two decreases. This result is to be expected since the first- and higher-order routes are far more well-mixed than the direct zeroth-order route from the source to the sink. Thus, with decreasing η_{ef} , the indirect routes make increasing contributions, thus making the well-mixed assumption more appropriate.

IX. CONCLUSIONS

We propose a statistical framework to address the effects of recycling and filtration on the concentration of airborne virus-laden droplet nuclei within indoor spaces ventilated by an air-conditioning unit. We applied the framework to a canonical room of size $10 \times 10 \times 3.2 \,\mathrm{m}^3$ with a four-way cassette air-conditioning system placed at the center of the ceiling. We use large eddy simulations (LES) to solve for the turbulent flow field and showcase results for ACH (air changes per hour) values of 2.5 and 5. We follow Salinas *et al.*²⁴ and implement a statistical overloading technique by individually tracking 20×10^6 droplet nuclei of size ranging from r = 0.1 to $r = 50 \,\mu\mathrm{m}$. One of the main objectives of the framework is to evaluate the concentration of droplet nuclei near a receiving host (i.e., the sink) that were ejected by an expiratory activity (i.e., talking, breathing, singing, etc.) of an infected individual (i.e., the source), where both the source and the sink may be located anywhere in the room.

A key aspect of the framework is to recognize that droplet nuclei may travel from the source to the sink either directly (i.e., without passing through the ventilation system) or indirectly by first leaving the room through the ventilation outlet and then reentering the room through the inlet before reaching the sink. In fact, droplet nuclei may recycle through the ventilation system multiple times before reaching the sink. We, therefore, divide the trajectory into four building blocks elementary processes (Ep1 through Ep4) that can be combined to provide a statistical description for the path that nuclei take from any source location to any sink location. Ep1 refers to the direct path from the source to the sink (i.e., without passing through the ventilation system), Ep2 refers to the path from the source to the outlet, Ep3 refers to the path from the inlet to the outlet, and Ep4 refers to the path from the inlet to the sink. By combining the elementary processes, along with the appropriate recycling/filtration efficiency, the zeroth order direct route that does not pass through the air-conditioning unit, and the first-, second-, and higher-order routes that do pass through the air-conditioning unit once, twice, and many times can be reconstructed. These routes can then be added together to evaluate the droplet nuclei concentration at the sink location for any recycling/filtration efficiency.

The proposed framework is designed to be used with the well-mixed model by providing an easy-to-implement correction function to the well-mixed model to produce statistically reliable risk assessments for viral transmission in indoor settings. The correction function primarily accounts for the source-to-sink separation distance, and accurately predicts the increase in the droplet nuclei concentration at smaller separation distances and substantially lower concentrations at larger separation distances. It should be borne in mind that whether separation distances are short or large, they must be considered relative to the room size, i.e., a 1 m separation distance in a small room, might correspond to a 2 m separation in a similar room that is eight times larger by volume, and so on. The correction function is observed to depend on time and filtration efficiency, but fortunately, it is largely independent of ACH and expiratory activity.

While the nuclei concentration within the room for the direct path was observed to depart substantially from the well-mixed approximation, especially at short source-to-sink scaled separations, ²⁴ the recycled nuclei, i.e., nuclei reentering the room through the inlet, are relatively well-approximated by the well-mixed model, especially those with smallest sizes. This well-mixedeness of the recycled nuclei is observed to reduce the magnitude of the correction. Two case studies were performed to assess the importance of filtration as well as departure from well-mixedness. The case studies consisted of a typical classroom and a nursing home. It was found that using proper filtration can increase the cumulative exposure time in typical classroom settings by up to four times and could allow visitations to nursing homes for up to 45 min.

Future studies should consider various room geometries (different size, aspect ratio, shape, etc.) and ventilation systems (different placement, one-way vs four-way cassettes, multiple outlets, etc.) to investigate their effects specifically on the correction function. Other studies could also investigate the use of portable filtration devices, their optimal location, and influence on indoor pathogen concentration.

ACKNOWLEDGMENTS

We gratefully acknowledge the support from NSF (EAGER Grant No. 2134083), LG Electronics (Grant No. C2021017165), and the University of Florida Informatics Institute.

AUTHOR DECLARATIONS Conflict of Interest

The authors have no conflicts to disclose.

Author Contributions

K. A. Krishnaprasad: Conceptualization (equal); Data curation (lead);
 Formal analysis (lead); Investigation (lead); Methodology (lead);
 Visualization (equal); Writing – review & editing (supporting). Jorge S.
 Salinas: Conceptualization (equal). Nadim Zgheib: Conceptualization (equal);
 Project administration (equal); Supervision (equal);
 Writing – review & editing (equal).
 S. Balachandar: Conceptualization (equal);
 Funding acquisition (equal);
 Methodology (equal);
 Supervision (equal);
 Writing – original draft (lead);
 Writing – review & editing (equal).

DATA AVAILABILITY

The data that support the findings of this study are available from the corresponding author upon reasonable request.

REFERENCES

- ¹R. Zhang, Y. Li, A. L. Zhang, Y. Wang, and M. J. Molina, "Identifying airborne transmission as the dominant route for the spread of COVID-19," Proc. Natl. Acad. Sci. 117, 14857 (2020).
- ²Y. Liu, A. A. Gayle, A. Wilder-Smith, and J. Rocklöv, "The reproductive number of COVID-19 is higher compared to SARS coronavirus," J. Travel Med. 27, taaa021 (2020).
- ³A. Foster and M. Kinzel, "Estimating COVID-19 exposure in a classroom setting: A comparison between mathematical and numerical models," Phys. Fluids 33, 021904 (2021).
- ⁴V. Vuorinen, M. Aarnio, M. Alava, V. Alopaeus, N. Atanasova, M. Auvinen, N. Balasubramanian, H. Bordbar, P. Erästö, R. Grande et al., "Modelling aerosol transport and virus exposure with numerical simulations in relation

- to SARS-CoV-2 transmission by inhalation indoors," Saf. Sci. 130, 104866 (2020).
- ⁵K. L. Chong, C. S. Ng, N. Hori, R. Yang, R. Verzicco, and D. Lohse, "Extended lifetime of respiratory droplets in a turbulent vapor puff and its implications on airborne disease transmission," Phys. Rev. Lett. **126**, 034502 (2021).
- ⁶M. Abkarian and H. A. Stone, "Stretching and break-up of saliva filaments during speech: A route for pathogen aerosolization and its potential mitigation," Phys. Rev. Fluids 5, 102301 (2020).
- ⁷A. Fabregat, F. Gisbert, A. Vernet, S. Dutta, K. Mittal, and J. Pallarès, "Direct numerical simulation of the turbulent flow generated during a violent expiratory event," Phys. Fluids 33, 035122 (2021).
- ⁸A. Fabregat, F. Gisbert, A. Vernet, J. A. Ferré, K. Mittal, S. Dutta, and J. Pallarès, "Direct numerical simulation of turbulent dispersion of evaporative aerosol clouds produced by an intense expiratory event," Phys. Fluids 33, 033329 (2021).
- ⁹V. Mathai, A. Das, J. A. Bailey, and K. Breuer, "Airflows inside passenger cars and implications for airborne disease transmission," Sci. Adv. 7, eabe0166 (2021).
- ¹⁰M. Z. Bazant, O. Kodio, A. E. Cohen, K. Khan, Z. Gu, and J. W. Bush, "Monitoring carbon dioxide to quantify the risk of indoor airborne transmission of COVID-19," Flow 1, E10 (2021).
- ¹¹M. Kanso, M. Naime, V. Chaurasia, K. Tontiwattanakul, E. Fried, and A. J. Giacomin, "Coronavirus pleomorphism," Phys. Fluids 34, 063101 (2022).
- ¹²M. C. Pak, R. Chakraborty, M. Kanso, K. Tontiwattanakul, K.-I. Kim, and A. J. Giacomin, "Coronavirus peplomer interaction," Phys. Fluids 34, 113109 (2022).
- ¹³C. Axfors and J. P. Ioannidis, "Infection fatality rate of COVID-19 in community-dwelling populations with emphasis on the elderly: An overview," medRxiv (2021).
- ¹⁴V. Senatore, T. Zarra, A. Buonerba, K.-H. Choo, S. W. Hasan, G. Korshin, C.-W. Li, M. Ksibi, V. Belgiorno, and V. Naddeo, "Indoor versus outdoor transmission of SARS-COV-2: Environmental factors in virus spread and underestimated sources of risk," Euro-Mediterr. J. Environ. Integr. 6, 30 (2021).
- ¹⁵B. R. Rowe, A. Canosa, J.-M. Drouffe, and J. Mitchell, "Simple quantitative assessment of the outdoor versus indoor airborne transmission of viruses and COVID-19," Environ. Res. 198, 111189 (2021).
- ¹⁶R. K. Bhagat, M. D. Wykes, S. B. Dalziel, and P. Linden, "Effects of ventilation on the indoor spread of COVID-19," J. Fluid Mech. 903, F1 (2020).
- ¹⁷S. Moritz, C. Gottschick, J. Horn, M. Popp, S. Langer, B. Klee, O. Purschke, M. Gekle, A. Ihling, F. D. Zimmermann *et al.*, "The risk of indoor sports and culture events for the transmission of COVID-19," Nat. Commun. 12, 5096 (2021).
- 18. Z. Peng, A. P. Rojas, E. Kropff, W. Bahnfleth, G. Buonanno, S. J. Dancer, J. Kurnitski, Y. Li, M. G. Loomans, L. C. Marr et al., "Practical indicators for risk of airborne transmission in shared indoor environments and their application to COVID-19 outbreaks," Environ. Sci. Technol. 56, 1125 (2022).
- ¹⁹B. Blocken, T. van Druenen, A. Ricci, L. Kang, T. van Hooff, P. Qin, L. Xia, C. A. Ruiz, J. Arts, J. Diepens *et al.*, "Ventilation and air cleaning to limit aerosol particle concentrations in a gym during the COVID-19 pandemic," Build. Environ. 193, 107659 (2021).
- ²⁰L. Schibuola and C. Tambani, "High energy efficiency ventilation to limit COVID-19 contagion in school environments," Energy Build. 240, 110882 (2021).
- ²¹P. Li, C. Wang, Y. Zhang, and F. Wei, "Air filtration in the free molecular flow regime: A review of high-efficiency particulate air filters based on carbon nanotubes," Small 10, 4543 (2014).
- ²²W. J. Fisk and D. Faulkner, "Performance and cost of particle air filtration technologies," <u>Indoor Air 12</u>, 223 (2001).
- ²³M. Z. Bazant and J. W. Bush, "A guideline to limit indoor airborne transmission of covid-19," Proc. Natl. Acad. Sci. 118, e2018995118 (2021).
- ²⁴J. S. Salinas, K. Krishnaprasad, N. Zgheib, and S. Balachandar, "Improved guidelines of indoor airborne transmission taking into account departure from the well-mixed assumption," Phys. Rev. Fluids 7, 064309 (2022).
- 25W. Wells, "Airborne contagion and air hygiene: An ecological study of droplet infections," J. Amer. Med. Assoc. 159, 90 (1955).
- ²⁶E. Riley, G. Murphy, and R. Riley, "Airborne spread of measles in a suburban elementary school," Am. J. Epidemiol. 107, 421 (1978).

- ²⁷K. McAuley, J. Talbot, and T. Harris, "A comparison of two-phase and well-mixed models for fluidized-bed polyethylene reactors," Chem. Eng. Sci. 49, 2035 (1994).
- ²⁸K. S. Pang, Y. R. Han, K. Noh, P. I. Lee, and M. Rowland, "Hepatic clearance concepts and misconceptions: Why the well-stirred model is still used even though it is not physiologic reality?," Biochem. Pharmacol. 169, 113596 (2019).
- ²⁹H. Hottel, G. Williams, and A. Bonnell, "Application of well-stirred reactor theory to the prediction of combustor performance," Combust. Flame 2, 13–34 (1958)
- ³⁰C. Van Heerden, A. Nobel, and D. Van Krevelen, "Mechanism of heat transfer in fluidized beds," Ind. Eng. Chem. 45, 1237 (1953).
- ³¹P. Moin, "Advances in large eddy simulation methodology for complex flows," Int. J. Heat Fluid Flow 23, 710 (2002).
- ³²S. Balachandar and J. K. Eaton, "Turbulent dispersed multiphase flow," Annu. Rev. Fluid Mech. 42, 111 (2010).
- ³³J. Wilson, S. Miller, and D. Mukherjee, "A Lagrangian approach towards quantitative analysis of flow-mediated infection transmission in indoor spaces with application to SARS-COV-2," Int. J. Comput. Fluid Dyn. 35, 727–742 (2021).
- ³⁴J. Capecelatro and O. Desjardins, "An Euler-Lagrange strategy for simulating particle-laden flows," J. Comput. Phys. 238, 1-31 (2013).
 ³⁵S. Balachandar, K. Liu, and M. Lakhote, "Self-induced velocity correction for
- 35S. Balachandar, K. Liu, and M. Lakhote, "Self-induced velocity correction for improved drag estimation in Euler-Lagrange point-particle simulations," J. Comput. Phys. 376, 160 (2019).
- ³⁶M. Germano, U. Piomelli, P. Moin, and W. H. Cabot, "A dynamic subgrid-scale eddy viscosity model," Phys. Fluids A 3, 1760 (1991).
- ³⁷D. K. Lilly, "A proposed modification of the Germano subgrid-scale closure method," Phys. Fluids A 4, 633 (1992).
- ³⁸M. O. Deville, P. F. Fischer, P. F. Fischer, E. Mund et al., High-Order Methods for Incompressible Fluid Flow (Cambridge University Press, 2002), Vol. 9.
- ³⁹F. Q. Hu, "On absorbing boundary conditions for linearized Euler equations by a perfectly matched layer," J. Comput. Phys. 129, 201 (1996).
- ⁴⁰ M. Allahyari, K. Liu, J. Salinas, N. Zgheib, and S. Balachandar, "Sensitivity of puff dynamics and airborne droplet nuclei distribution to variations in violent expiration events," Comput. Fluids 251, 105758 (2022).
- ⁴¹K. Liu, M. Allahyari, J. Salinas, N. Zgheib, and S. Balachandar, "Investigation of theoretical scaling laws using large eddy simulations for airborne spreading of viral contagion from sneezing and coughing," Phys. Fluids 33, 063318 (2021).
- ⁴²K. Liu, M. Allahyari, J. S. Salinas, N. Zgheib, and S. Balachandar, "Peering inside a cough or sneeze to explain enhanced airborne transmission under dry weather," Sci. Rep. 11, 9826 (2021).
- 43M.-R. Pendar and J. C. Páscoa, "Numerical modeling of the distribution of virus carrying saliva droplets during sneeze and cough," Phys. Fluids 32, 083305 (2020).
- ⁴⁴P. Katre, S. Banerjee, S. Balusamy, and K. C. Sahu, "Fluid dynamics of respiratory droplets in the context of COVID-19: Airborne and surfaceborne transmissions," Phys. Fluids 33, 081302 (2021).
- ⁴⁵L. Morawska, G. Johnson, Z. Ristovski, M. Hargreaves, K. Mengersen, S. Corbett, C. Y. H. Chao, Y. Li, and D. Katoshevski, "Size distribution and sites

- of origin of droplets expelled from the human respiratory tract during expiratory activities." I. Aerosol Sci. 40, 256 (2009).
- 46T. Dbouk and D. Drikakis, "On coughing and airborne droplet transmission to humans." Phys. Fluids 32, 053310 (2020).
- ⁴⁷J. Pozorski and J.-P. Minier, "On the Lagrangian turbulent dispersion models based on the Langevin equation," Int. J. Multiphase Flow 24, 913 (1998).
- ⁴⁸P. Fede, O. Simonin, P. Villedieu, and K. Squires, "Stochastic modeling of the turbulent subgrid fluid velocity along inertial particle trajectories," in *Proceedings of the Summer Program* (Center for Turbulence Research, 2006), pp. 247–258.
- ⁴⁹K. Liu, P. Huck, A. Aliseda, and S. Balachandar, "Investigation of turbulent inflow specification in Euler-Lagrange simulations of mid-field spray," Phys. Fluids 33, 033313 (2021).
- ⁵⁰A. Dehbi, "Turbulent particle dispersion in arbitrary wall-bounded geometries: A coupled CFD-Langevin-equation based approach," Int. J. Multiphase Flow 34, 819 (2008).
- 51 A. A. Mofakham and G. Ahmadi, "Particles dispersion and deposition in inhomogeneous turbulent flows using continuous random walk models," Phys. Fluids 31, 083301 (2019).
- ⁵²J. Ferry and S. Balachandar, "A fast Eulerian method for disperse two-phase flow," Int. J. Multiphase Flow 27, 1199 (2001).
- ⁵³D. Zwick and S. Balachandar, "A scalable Euler-Lagrange approach for multiphase flow simulation on spectral elements," Int. J. High Perform. Comput. Appl. 34, 316 (2020).
- 54S. Balachandar, S. Zaleski, A. Soldati, G. Ahmadi, and L. Bourouiba, "Host-to-host airborne transmission as a multiphase flow problem for science-based social distance guidelines," Int. J. Multiphase Flow 132, 103439 (2020).
- 55Y. Bu, R. Ooka, H. Kikumoto, and W. Oh, "Recent research on expiratory particles in respiratory viral infection and control strategies: A review," Sustainable Cities Soc. 73, 103106 (2021).
- ⁵⁶B. Wang, H. Wu, and X.-F. Wan, "Transport and fate of human expiratory droplets—A modeling approach," Phys. Fluids 32, 083307 (2020).
- 57X. Yang, C. Ou, H. Yang, L. Liu, T. Song, M. Kang, H. Lin, and J. Hang, "Transmission of pathogen-laden expiratory droplets in a coach bus," J. Hazard. Mater. 397, 122609 (2020).
- ⁵⁸J. Wang, M. Alipour, G. Soligo, A. Roccon, M. De Paoli, F. Picano, and A. Soldati, "Short-range exposure to airborne virus transmission and current guidelines," Proc. Natl. Acad. Sci. 118, e2105279118 (2021).
 ⁵⁹S. L. Miller, W. W. Nazaroff, J. L. Jimenez, A. Boerstra, G. Buonanno, S. J.
- S. L. Miller, W. W. Nazaroff, J. L. Jimenez, A. Boerstra, G. Buonanno, S. J. Dancer, J. Kurnitski, L. C. Marr, L. Morawska, and C. Noakes, "Transmission of SARS-CoV-2 by inhalation of respiratory aerosol in the Skagit Valley Chorale superspreading event," Indoor Air 31, 314 (2021).
- ⁶⁰G. Buonanno, L. Stabile, and L. Morawska, "Estimation of airborne viral emission: Quanta emission rate of SARS-CoV-2 for infection risk assessment," Environ. Int. 141, 105794 (2020).
- ⁶¹G. Buonanno, L. Morawska, and L. Stabile, "Quantitative assessment of the risk of airborne transmission of SARS-CoV-2 infection: Prospective and retrospective applications," Environ. Int. 145, 106112 (2020).